Nano Energy 81 (2021) 105647

Contents lists available at ScienceDirect

Nano Energy

journal homepage: http://www.elsevier.com/locate/nanoen

Review

Water droplet bouncing dynamics

Xingjian Yu, Yu Zhang, Run Hu *, Xiaobing Luo *

State Key Laboratory for Coal Combustion, School of Energy and Power Engineering, Huazhong University of Science and Technology, Wuhan 430074, China

ARTICLE INFO

Keywords:
Water droplet
Bouncing dynamics
Surface topography
Surface technologies

ABSTRACT

Droplet bouncing on surfaces has long been observed in nature and industry, which is rather intriguing and instructive for related technology development. Recent decades have witnessed significant progress on the mechanism exploring, device development, and application demonstrations. In this review, we focus on the recent progresses that aim at introducing the phenomena, revealing the underlying physics, and promoting the potential applications of water droplet bouncing on various solid and soft surfaces like hydrophobic/hydrophilic/heated solid surfaces and liquid film/bath/droplet. The water droplet bouncing dynamics is highly dependent on the liquid properties, surface characteristics and ambient pressure. The absence of droplet/surface contact, as the key point for droplet bouncing, can be realized by lowering the Weber number of droplet and designing hydrophobic surfaces to reduce the droplet-surface contact, actively maintaining the air/vapor film by heating the solid surface above the Leidenfrost point, vibrating the liquid bath, applying electric/magnetic/pressure fields, etc. Moreover, the comprehensive understanding of droplet bouncing has promoted the development of numerous advanced surfaces technologies, including surface self-cleaning, directional droplet transportation, heat transfer enhancement, droplet logic gate, electrical generation and so on. Finally, the future directions for research and application are outlined and discussed.

1. Introduction

Water droplets impact on surfaces is an intriguing phenomenon that involves complicated physical mechanisms and has inspired the droplet-related technology development in industry for a long time [1–4]. In nature, raindrop impact on stones, soils, plant leaves and liquid pools are so common phenomena that we may even pay no attention to them in our daily lives. In industry, there are also droplet-wall interactions in surface coating, surface cleaning, electronics cooling, fire extinguishing, direct fuel injection combustion, metal quenching, inkjet printing and so on. In general, water droplet impact on surfaces may undergo depositing, boiling, splashing and bouncing behaviors depending on the specific conditions [5–11]. The first three behaviors happen more frequently, while the droplet bouncing is relatively rare to happen as it requires more rigorous conditions including the droplet properties (viscosity, surface tension, radius, etc.), surface characteristics (wettability, roughness, topography, temperature, thermal conductivity, etc.) and ambient conditions (pressure, temperature, etc.) [5–11]. It is reported that the droplet bouncing can happen on both solid and liquid surfaces, and the essence is the presence of stable air/vapor film beneath the droplet to prevent the droplet from wetting the surfaces or coalescing with other liquids. The stable air/vapor film could only be achieved at some rigorous conditions, such as extremely low Weber number ($We = \rho v^2 R/\gamma$, where ρ, v, R and γ represent the density, impact velocity, radius and surface tension of the droplet.), hydrophobic surfaces with elaborate surface topography, heated surfaces with surface temperature above the Leidenfrost point, and vertically vibrated liquid baths. Therefore, the research of droplet bouncing is more attracting and involves very complex physical mechanisms, including surface wettability, surface topography, interfacial tensions, droplet/air/vapor deformation and so on.

However, it is until recent decades that the underlying physics behind water droplet bouncing was partly revealed due to the rapid development of 3D micro-nano imaging technology, high-speed video measurement technology, surface processing technology and numerical modeling methods [5–11]. With the 3D micro-nano imaging technology, such as scanning electron microscope (SEM), transmission electron microscope (TEM) and atomic force microscope (AFM), the surface topography of the surfaces can be clearly observed. The complicated micro-/nano-texture on natural surfaces, such as lotus leaf, has inspired the researchers to design bio-inspired surfaces with advanced surface processing technology for manipulating the water droplet bouncing

* Corresponding authors.
E-mail addresses: hurun@hust.edu.cn (R. Hu), luoxb@hust.edu.cn (X. Luo).

https://doi.org/10.1016/j.nanoen.2020.105647
Received 20 October 2020; Received in revised form 18 November 2020; Accepted 27 November 2020
Available online 1 December 2020

behaviors. With the high-speed video measurement technology and numerical modeling methods, the deformation of droplet/air/vapor can be clearly characterized to explain the mechanisms behind water droplet bouncing. Armed with these advanced tools, water droplet bouncing, as one of the typical phenomena of droplet impact dynamics, has attracted extensive attentions and interests in recent decades. Specifically, the water droplet bouncing dynamics on hydrophobic/hydrophilic/heated surfaces and liquid droplet/film/bath was widely investigated to reveal the effect of droplet properties, surface characteristics and ambient conditions on the droplet/air/vapor deformation, bouncing height, moving speed, contact time and energy transformation [5–11]. The recent progresses on droplet bouncing are so attractive and significant that they reveal the underlying physics of droplet-surface interactions, and promote the development of numerous advanced applications, including surface self-cleaning [1–3], droplet transportation [12–14], spraying cooling [15–20] and so on. As far as we are concerned, water droplet bouncing, though emerging with significant progress and important applications, has rarely been reviewed comprehensively and systematically to highlight the significance, summarize the progress, and outline the development directions yet.

In this review, water droplet bouncing dynamics is comprehensively reviewed including the bouncing phenomena, the underlying theories and the potential applications. The organization of this review is summarized in Fig. 1. In Section 2, the theories of droplet bouncing will be introduced, including surface wettability, interfacial tensions, surface roughness and droplet/vapor/air deformation. In addition, the experimental and numerical methods for characterizing the droplet bouncing dynamics will also be introduced in this section. In Section 3, several typical droplet bouncing dynamics will be reviewed, including droplet bouncing on hydrophobic/hydrophilic/heated solid surfaces and liquid film/bath/droplet. In Section 4, some advanced applications inspired by the droplet bouncing dynamics will be introduced, including surface self-cleaning, directional droplet transportation, heat transfer enhancement, droplet logic gates and electrical generation. In Section 5, the future directions for both research and application are outlined.

2. Theories and methods

When a droplet impacts on the surfaces, the droplet/air/vapor undergoes larger deformation in a flash due to the dynamic wetting phenomenon at the three-phase contact line. Bouncing happens when a stable vapor layer forms beneath the droplet, and the formation of vapor layer depends on the interplay of surface wettability, interfacial tensions and surface topography. In this section, theories and methods that related to droplet bouncing are introduced, including the basis of surface wetting and experimental/numerical methods for characterizing the droplet/air/vapor deformation during droplet bouncing process.

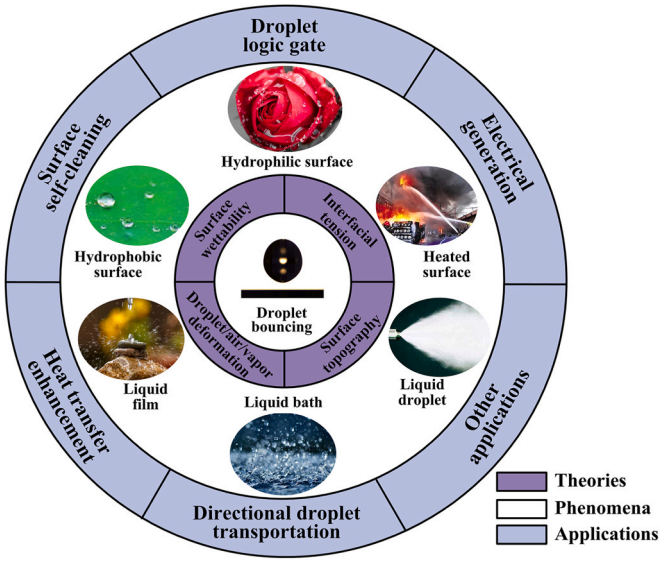

Fig. 1. A schematic summary of the theories, phenomena and applications of droplet bouncing.

2.1. Basis of surface wetting

When a droplet impacts on a smooth surface shown as Fig. 2(a), its equilibrium CA θ is given by the well-known Young's equation as [21]:

$$\gamma_{SV} = \gamma_{LV}\cos\theta + \gamma_{SL} \tag{1}$$

where γ_{SV}, γ_{SL}, and γ_{LV} represent the interfacial tension of the solid-vapor, solid-liquid and liquid-vapor interfaces. The γ_{SV} and γ_{LV} are commonly known as surface energy of solid surface and surface tension of liquid. According to the θ of water, a surface can be divided into super-hydrophilic ($\theta < 5°$), hydrophilic ($\theta < 90°$), hydrophobic ($\theta > 90°$) and super-hydrophobic ($\theta > 150°$), and the droplet tends to bounce off the hydrophobic surfaces.

The Young's equation shows that the θ can be enlarged by increasing the γ_{LV} and decreasing the γ_{SV}, which benefits for triggering the droplet bouncing. However, limited by the γ_{LV} of common liquids and γ_{SV} of common solids [22–25], the reported maximum θ of a water droplet on the smooth surface is ~130° [26,27]. Introducing elaborate surface topography was confirmed to be an effective way to further decrease or increase the θ, depending on the dimension/geometry/arrangement of the surface topography and the wetting state of the droplet [1–4]. However, the Young's equation is only suitable for smooth surfaces. Under this situation, the Wenzel and Cassie-Baxter wetting states were proposed. For the Wenzel wetting state shown as Fig. 2(b), the liquid fully wets the surface topography and the apparent CA θ^* can be calculated by the Wenzel equation as [13]:

$$\cos\theta^* = r\cos\theta \tag{2}$$

Where the r represents the roughness of the surfaces, which is defined as the ratio of the actual surface area to the geometrically projected surface area. The r is always larger than 1, so the surface roughness amplifies both hydrophilic and hydrophobic properties in Wenzel wetting state, which means $\theta^* << 90°$ if $\theta < 90°$ and $\theta^* << 90°$ if $\theta > 90°$.

For the Cassie-Baxter wetting state shown as Fig. 2(c), the liquid partially wets the surface topography and the apparent CA θ^* is determined by the Cassie-Baxter equation as [13]:

$$\cos\theta^* = f\cos\theta + f - 1 \tag{3}$$

where f is the area fraction of the solid–liquid interface in the vicinity of the triple phase contact line. It can be derived from Eq. (3) that for

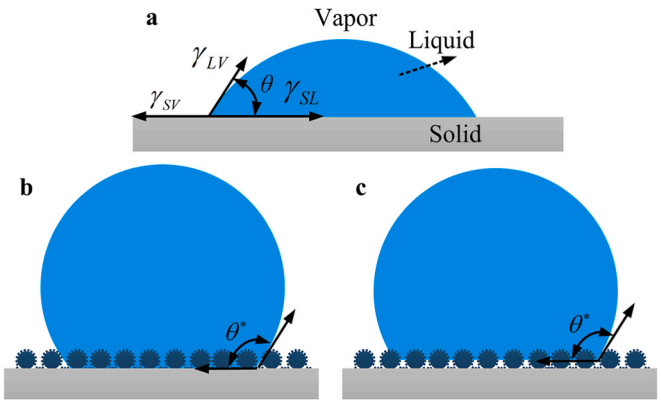

Fig. 2. Equilibrium geometry of droplet on (a) smooth surface and rough surfaces in (b) Wenzel wetting state and (c) Cassie-Baxter wetting state.

droplet in Cassie-Baxter wetting state, θ^* is always larger than θ. Compared to the Wenzel wetting state, the formation of Cassie-Baxter wetting state rises possibility for increasing the θ^* of hydrophilic surface and leads to very high θ^* for hydrophobic surface.

Although the Wenzel and Cassie-Baxter equations are well known and widely applied, they do not take a deep look into the surface topography. The surface roughness is an overall characterization of the surface, while the surface topography plays a dominant role in deciding the local wetting state of liquid [1–4]. In fact, the elaborate surface topography could be more important than the overall surface roughness for droplet impact in certain conditions [23,28]. Inspired by the surface topographies of natural hydrophobic surfaces, numerous advanced surface processing technologies were developed to construct artificial hydrophobic and hydrophilic surfaces with milli/micro/nano hierarchical surface topographies [1–4,13,23,28–30], including etching, lithography, anodization, electrospun, vapor-deposition, micro/-nanoparticle deposition, spray/dip coating and so on. Furthermore, by modifying the rough surfaces with low surface energy materials, the surfaces can present high-repellence to liquid with both high and low surface tension [23,28].

2.2. Experimental methods

The droplet bouncing, in which the droplet is separated from the surface by a (sub)micrometer air/vapor film, happens in a flash with contact time of tens or even just several milliseconds, so human eyes and conventional charge coupled device (CCD) camera are difficult to clearly observe the droplet/air/vapor deformation. Until recent decades, the rapid development of high-speed camera with frame speed higher than 1000 fps helps researcher to clearly observe the droplet bouncing dynamics. The deformation of droplet can be easily observed from side/top views. However, the deformation of air/vapor should be observed from bottom view, which requires very precise optical systems. Therefore, combining the high-speed camera and the precise optical systems, several high-speed video measurement technologies were developed.

Fig. 3(a) schematically shows the high-speed video measurement systems for observing the droplet deformation from top/side views. The high-speed camera is placed at the top/side directions of droplet, while the high-power light source is placed along with or opposite to the high-speed camera. With these systems, the droplet impact dynamics, including the droplet deformation, triple phase contact line, contact time and evaporation time, can be fully analyzed.

Compared to the droplet deformation observation, the air/vapor deformation observation is far difficult. Firstly, the thickness of the air/vapor film could reduce to sub-micrometer during the droplet-surface contact. Secondly, the air/vapor is embedded in the bottom of droplet. To capture the air/vapor deformation beneath the droplet, high-speed video measurement systems based on interference [31–33] and reflection [34,35] methods were developed. For the interference method shown as Fig. 3(b), a collimating laser beam shines at the bottom of the surface. The reflected light from the liquid–vapor and vapor–solid interfaces interfere either constructively or destructively to form interference fringes. A semi-transparent mirror with tilting angle of 45° together with an interferometer filter are applied to visualize the interference fringes. The interference method is feasible to measure the thickness of the air/vapor film. However, it presents low sensitivity to the triple phase contact line, so it is not suitable to capture the geometry of air/vapor film for some complicated liquid-vapor interfaces [31–33]. For the reflection method shown as Fig. 3(c), a collimating laser beam shine at the bottom of the surface with an incident angle θ_c. The θ_c should be adjusted to between the critical total internal reflection angle of solid-liquid interface θ_{SL} and solid-vapor interface θ_{SV}, so that the incident light would be reflected at the solid-vapor interface while penetrates the solid-liquid interface. As a result, the recorded images have dark spots (solid-liquid interface) and bright spots (solid-vapor interface). The reflection method is not suitable to measure the thickness of the air/vapor film. However, it presents high sensitivity to the triple phase contact line, so it is better than the interference method in revealing the geometry of air/vapor film [34,35].

2.3. Numerical methods

Although experiment characterizations are the popular method to explore the phenomena and mechanism of droplet bouncing dynamics, they are not applicable at some practical scenarios. Firstly, the existing high-speed video measurement systems are difficult to detect the air/vapor profile on rough or opaque surfaces. Secondly, the droplet/air/vapor deformation at the three-phase contact line depends on the droplet evaporation, air/vapor compression, pressure inside the air/vapor layer and interplay of gravity, inertial, viscous, interfacial and Van der Waals forces, which is hard to be analyzed by experiments. To tackle these difficulties faced by the experiments, as shown in Fig. 4, numerical modeling of droplet bouncing based on computational fluid dynamics (CFD), lattice Boltzmann method (LBM) and molecular dynamics (MD)

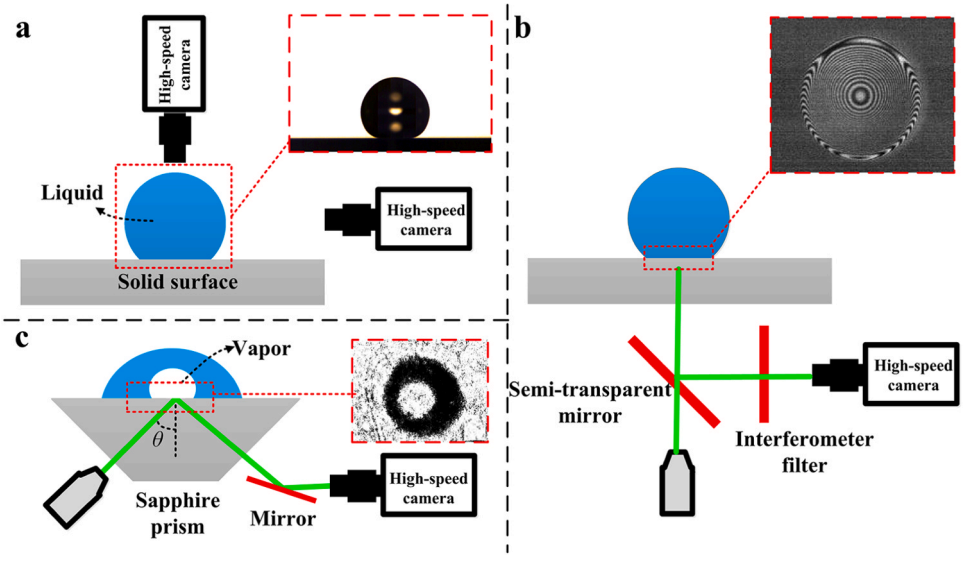

Fig. 3. Schematic of the high-speed video measurement systems for (a) observing the droplet deformation from top/side views and observing deformation of air/vapor film from bottom view based on (b) interference [31] and (c) reflection method.

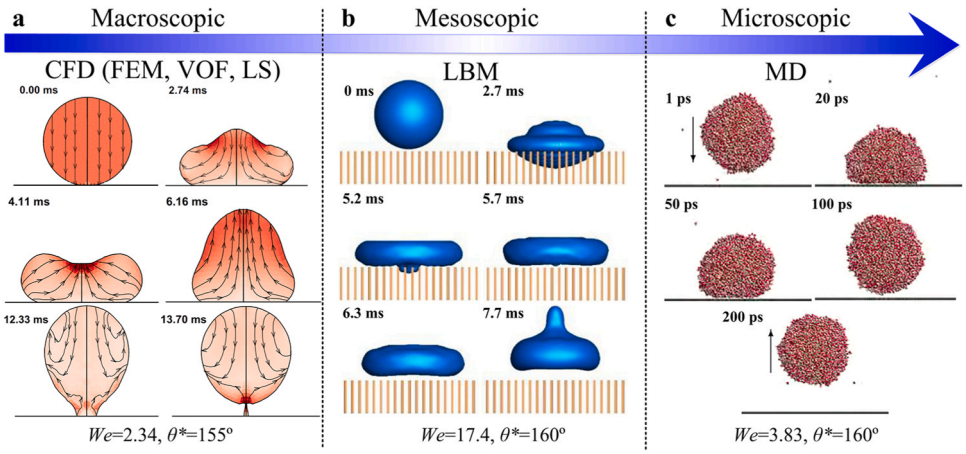

Fig. 4. Numerical modeling for droplet bouncing. (a) FEM simulation [37], (b) LBM simulation [47] and (c) MD simulation [49].

are developed for macroscopic, mesoscopic, and microscopic simulations respectively.

The CFD method is the most widely used method for droplet modeling to trace the liquid-air/vapor interface with different techniques, such as finite element method (FEM) [36,37], volume of fluid (VOF) method [38–40], level-set (LS) method [41–43], coupled LS and VOF (CLSVOF) [44]. The FEM traces the liquid-air/vapor interface by using the Lagrangian objects such as particles, while the VOF and LS methods trace the liquid-air/vapor interface based on Eulerian framework. As a typical example of FEM-simulated droplet bouncing, Bange and Bhardwaj employed a FEM-based computational model to simulate the droplet bouncing dynamics and transient fluid flow inside the droplet on a super-hydrophobic surface with contact angle of 155° in Fig. 4(a) [37]. Their results indicate that the droplet bouncing is determined by the competition of the surface energy, inertial energy and gravitational energy at the moment of maximum recoiling droplet. The VOF method reconstructs the liquid-air/vapor interface by defining the volume fraction as 0 for air/vapor and as 1 for liquid, while the LS method traces the liquid-air/vapor interface by using a contour line function measured from the interface and is 0 at the interface. The CLSVOF was proposed to further improve the numerical accuracy by using the VOF to deal with the motion of liquid-air/vapor interface and using LS to deal with surface tension and wettability [44]. Furthermore, the refined grid was defined at the vicinity of the solid surface and droplet to capture the air layer beneath the droplet [38]. Khojasteh et al. used LS method to investigate the droplet bouncing dynamic on flat and curved hydrophobic and super-hydrophobic surfaces [43]. Their results show that the droplet on the curved surface presents larger maximum spreading diameter over that of the flat surface, while the contact time of the droplet is almost same on the flat and curved surfaces. In addition, the maximum spreading diameter and contact time of the droplet increase as the *We* increases.

The LBM is a mesoscopic modeling approach which can predict the mesoscopic droplet/air/vapor deformation. In addition, the LBM traces the liquid-air/vapor interface based on the density of the lattice nodes, which has higher accuracy over the CFD methods. Due to these two excellent advantages, LBM has attracted extensive attention and was treated as a promising alternative to simulate droplet bouncing on textured surfaces [45–48]. Zhang et al. developed a mesoscopic LBM model to explore the droplet bouncing dynamic on super-hydrophobic surface with randomly distributed texture, and the effect of roughness parameters (skewness and kurtosis) on the droplet bouncing abilities were discussed [45,46]. Yin et al. employed multiphase LBM method droplet bouncing dynamics on microtextured super-hydrophobic surfaces as shown in Fig. 4(b). Four possible bouncing types were identified, including conventional retracting bouncing, incomplete-retracting bouncing, impaled retracting bouncing and tumbling bouncing, and the droplet impact obliqueness promotes the incomplete-retracting bouncing and reduces the contact time thereby [47].

The MD method that simulates the molecular motion at femtosecond scale discloses the detailed mechanism of the droplet wetting and surface structure/chemistry. Therefore, it is an effective method to explore the microscopic droplet/air/vapor deformation [49–52]. Koishi et al. contacted MD simulations to investigate the nanodroplet bouncing condition for flat and nanopillared surfaces as shown in Fig. 4(c) [49]. Their results show that the droplet deformation has significant influence on the bouncing condition of droplets on the flat surfaces. The droplet bouncing condition shows weak dependence on the surface wettability if the droplet undergoes small deformation and shows strong dependence on the surface wettability if the droplet undergoes large deformation. However, for the nanopillared surfaces, the influence of droplet deformation on the droplet bouncing condition is relatively small because the surface hydrophobicity is enhanced due to the existence of pillars. Gao et al. employed MD method to simulate the coalescence-induced bouncing of nanodroplets on nanotextured surfaces, and the effect of droplet size, droplet number, surface wettability and texture density on the bouncing dynamic of nanodroplets were analyzed [50,51].

The aforementioned methods have their advantages and disadvantages from different aspects: (1) The CFD methods can easily capture the macroscopic droplet/air/vapor deformation. However, it is difficult to model the heterogeneous micro/nano boundary conditions. (2) The LBM has advantages in defining complex boundary conditions, so it rises possibility in modeling of heterogeneous micro/nano boundary conditions. However, the grid number required for LBM geometric model is extremely large, which hinders its application in large-scale modeling. (3) The MD reveals very detailed mechanism of droplet-surface interaction, which provides more useful information than the CFD and LBM. However, the computational load of MD is rather heavy even for tiny geometric model. Therefore, the MD is currently not suitable for studying real heterogeneous surfaces.

3. Droplet bouncing dynamics

With advanced experimental and numerical methods, droplet bouncing dynamics on various surfaces, like hydrophobic/hydrophilic/heated solid surfaces and liquid film/bath/droplet, were widely studied in recent decades. In this section, some typical droplet bouncing dynamics are reviewed in details, sorted by the impact target, triggering conditions and influencing parameters.

3.1. Bouncing on hydrophobic surfaces

Hydrophobic surfaces widely exist in nature as well as commonly used in industry, and droplet bouncing is a fundamental issue in the

practical application of hydrophobic surfaces [1–4]. Therefore, lots of experiments and simulations were conducted to study the droplet bouncing dynamics on the hydrophobic surfaces, including bouncing height, contact time and droplet deformation [7,10]. Among these bouncing dynamics parameters, the reduction of contact time is the key parameter as it influences the exchange of mass, momentum and energy between droplet and surface. The minimum contact time of a droplet on smooth hydrophobic surfaces is ~12 ms [53–55], while it could be reduced on rough hydrophobic surfaces, depending on the CA hysteresis (CAH), *We* and surface topography. Shen et al. found that the contact time of bouncing droplets on hydrophobic surfaces depends on the CAH significantly, and a minimum contact time of ~13 ms was observed for CAH of <5° [56]. Some researchers demonstrated that the contact time can be further reduced by breaking the symmetry spreading and receding of the bouncing droplet with asymmetric surface topography. In 2013, Bird et al. proposed a super-hydrophobic surface with macrotexture shown as Fig. 5(b) to redistribute the liquid mass and momentum, and thereby decrease the contact time to 7.8 ms shown as Fig. 5(c) [55]. In 2015, Shen et al. further enlarger such phenomenon by changing the dimension and arrangement of the macrotexture [57]. They found that the contact time of the droplet on surface with one-forked macrotexture is ~7.8 ms, which is close to the results obtained by Bird et al. However, they further found that the contact time decreases with the forked number shown as Fig. 5(d)–(g), and a minimum contact time of ~5.5 ms was observed with forked number larger than 5. By conducting a theoretical calculation, they demonstrated that ~5.5 ms is the minimum contact time of bouncing droplets on hydrophobic surfaces with macrotexture. In recent years, Wang's group designed two type of super-hydrophobic surfaces to reduce the contact time of bouncing droplet. One is curved super-hydrophobic surface, another is super-hydrophobic surface with truncated pyramidal posts shown as Fig. 6(a). The contact time reduction mechanism on the curved super-hydrophobic surface is similar to that reported by Bird et al. The droplet presents asymmetric bouncing along azimuthal and axial directions, and the contact times on the convex and concave super-hydrophobic surfaces are 11.8 ms and 10.3 ms, which are ~30% and ~40% smaller than that on the equivalent smooth surface (16.5 ms) [58,59]. However, the contact time reduction mechanism of droplet on the surface with truncated pyramidal posts is much different from that mentioned above. As shown in Fig. 6(b), the droplet penetrates the truncated pyramidal posts, and the capillary energy stored in the penetrated liquid is rectified into upward motion to lift up the droplet [60–63]. They have designed surfaces with straight posts and truncated pyramidal posts with half-apex angle of 1.0°, 1.7°, and 3.6° shown as Fig. 6(c)–(f). Compared with the surface with straight posts, the droplets leave the surfaces with truncated pyramidal posts in flattened, pancake shape without retracting shown as Fig. 6(g)-(j). By varying the *We*, a minimum contact time of ~3.4 ms was recorded shown as Fig. 6(k), which is the minimum contact time reported so far. In summary, the minimum contact times of droplet on the aforementioned hydrophobic surfaces are listed Table 1.

Along with the contact time, the effect of surface topography on the droplet deformation were also discussed. For surfaces with uniform surface topography and surface wettability shown as Fig. 7(a), the droplet spreads, recedes and rebounds radially shown as Fig. 7(b). In a recent study, surfaces with heterogeneous wettability and topography were applied to control the droplet bouncing dynamic. As shown in Fig. 7(c)–(e), Li et al. fabricated hydrophilic pattern (high-adhesive) on the hydrophobic surfaces (low-adhesive), the droplet recedes heterogeneously due to the exist of hydrophilic pattern and an interesting gyrating bouncing phenomenon happens [64]. Through mechanical modeling shown as Fig. 7(f)–(g), they found the rotating motion of the droplet is caused by the asymmetric adhesion forces that enabled by the surface heterogeneity. By optimizing the spiral radius *R* of the hydrophilic pattern, a maximum instantaneous rotational speed of >7300 revolutions per minute was captured shown as Fig. 7(h). In addition, the morphology of the grating droplet depends on the spiral number *N* shown as Fig. 7(i). Furthermore, they applied such a gyrating bouncing behavior to control the movement of the magnetically-levitated pyrolytic graphite (PG) flake with heterogeneous wettability shown as Fig. 7 (j). The water droplet impacts on the PG at *We* of 93 and forces the PG to rotate for more than 4000 ms shown as Fig. 7(k).

In the droplet bouncing dynamics that mentioned above, the bouncing height decreases monotonously with time due to the energy dissipation between the droplet and the air film. However, Schutzius et al. observed a spontaneous trampoline-like bouncing phenomenon on rough super-hydrophobic surface by reducing the ambient pressure to approximately 0.01 bar [65]. The droplet bouncing height increases after each collision, which indicates that the droplet gains energy from the droplet-vapor-surface interaction. As the droplet saturation

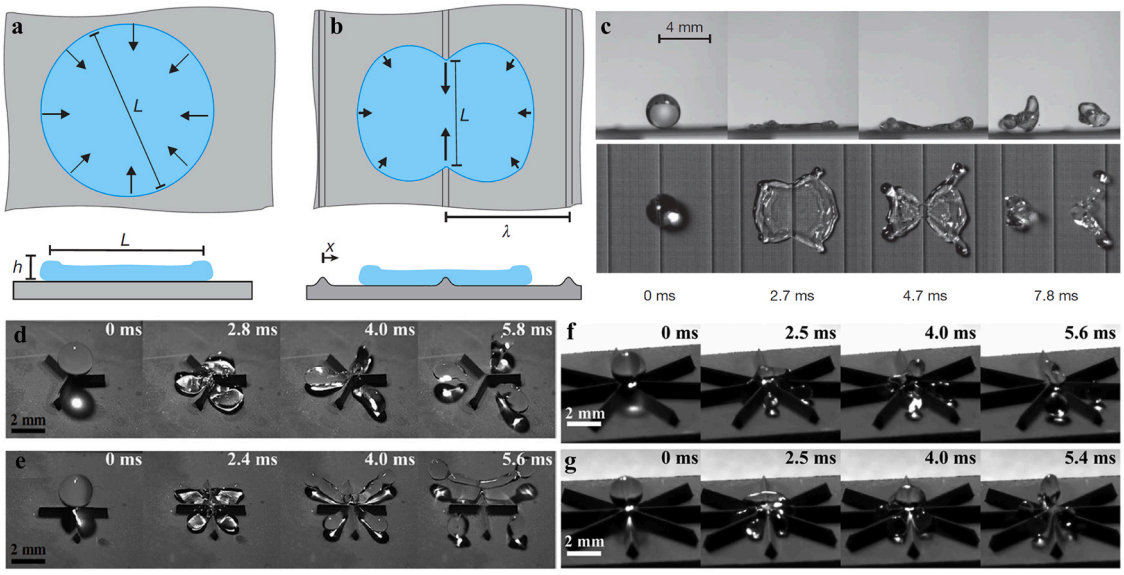

Fig. 5. Bouncing on super-hydrophobic surfaces with macrotexture. (a), (b) Schematic diagram of droplet retraction on surfaces with and without macrotexture, the macrotexture changes the thickness profile of the droplets and leads asymmetric recoil of droplet [55]. (c) Top and side views of droplet impact process on surface with macrotexture [55]. (d)–(g) Droplet impact on surfaces with 3, 4, 7, 8-forked macrotexture [57].

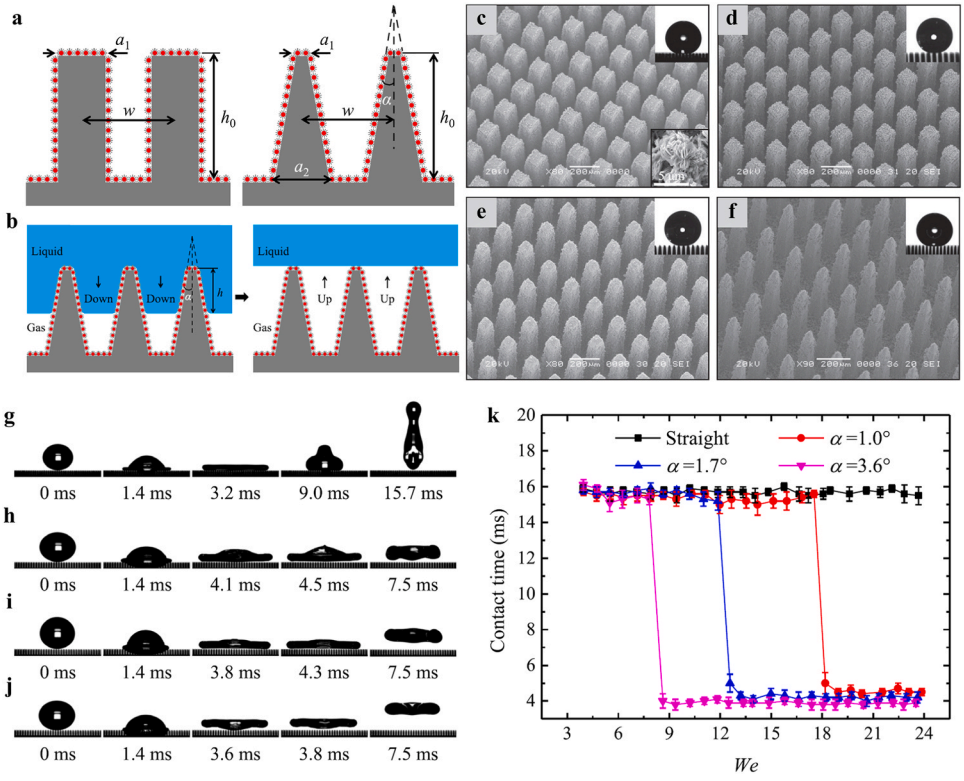

Fig. 6. Pancake bouncing on super-hydrophobic surfaces with truncated pyramidal post array [61]. (a) Schematic diagram of super-hydrophobic surfaces with straight post array and truncated pyramidal post array. (b) Schematic illustration of down penetration and up departure of water droplet on the truncated pyramidal posts. (c)–(f) Surface topography an wettability characterization of super-hy drophobic surfaces with (c) straight post array, truncated pyramidal posts with half-apex angle of (d) 1.0°, (e) 1.7°, and (f) 3.6°. (g)–(j) Droplet impact process on super-hydrophobic surfaces with (g) straight post array and truncated pyramidal posts with half-apex angle of (h) 1.0°, (i) 1.7°, and (j) 3.6°. (k) The relationship between contact time and *We* on the surfaces shown in (c)–(f).

Table 1
Minimum contact time of water droplet on various hydrophobic surfaces.

Surface type	CA	CAH	*We*	Minimum contact time	Ref.
Smooth polydimethylsiloxane (PDMS)	~107°		3.8	~12 ms	[54]
Laser-ablated silicon surface	~163°		~27	~12.4 ms	[55]
Micro/nanotextured titanium alloy	~161°	~2°	~14	~11.8 ms	[56, 57]
Surfaces with rosettes	~163°		7.9	~16.1 ms	[58]
Microtextured surfaces	~163°		~27	~7.8 ms	[55]
Micro/nanotextured titanium alloy	~161°	~2°	~14	~5.5 ms	[57]
Convex surface	~163°	~4°	7.9	~11.8 ms	[58]
Concave surface	~163°	~4°	7.9	~10.3 ms	[58]
Surface with straight post array	>165°	~2°	7.1	~16.5 ms	[60]
Surfaces with pyramidal post array	>165°	~2°	14.1	~3.4 ms	[60, 61]
Surfaces with porous networks	>160°		8.7	~4.5 mm	[45]

temperature decreases sharply with the ambient pressure, the droplet evaporates rapidly under extremely low ambient pressure. However, the surface adhesion and surface texture prevent the vapor from escaping from the droplet-surface contact region. As a result, the vapor accumulates beneath the droplet and generates high vapor pressure to levitate the droplet as well as increase the droplet momentum. They also show that the high vaporization rate of droplet under extremely low ambient pressure could induce droplet freezing and removing phenomenon, which might have broad application in surface anti-icing [65].

3.2. Bouncing on hydrophilic surfaces

As introduced in Section 3.1, droplets are easy to bounce off the hydrophobic surfaces due to the low droplet-surface contact area and entrapped air film within the surface topography. However, droplet bouncing on hydrophilic surfaces is rarely observed. When a droplet impacts on the hydrophilic surface, the droplet tends to fully wet the hydrophilic surface and its kinetic energy dissipates quickly due to the high surface adhesion caused by the low CA and high CAH of the surface [3]. As a result, the droplet fails to keep enough energy to bounce off the surface and splashing happens if the impact velocity (or *We*) is high enough.

It has been thought that the droplets cannot bounce on hydrophilic surfaces for a long time. Until recent years, the importance of air film in droplet-surface interaction was revealed and some researchers found that the droplets are able to bounce on hydrophilic surfaces by reducing the impact velocity of the droplet to <0.75 m/s (or $We < 4$) to squeeze a stable air film beneath the droplet [54,66–68]. Ruiter et al. demonstrated that droplets are able to bounce several times on hydrophilic surfaces when $We < 4$ due to the existence of a micro-thick air film. As shown in Fig. 8(a)–(d), droplet bouncing on hydrophilic glass surface was observed and a thin air layer was observed beneath the droplet. By analyzing the droplet/air film shape oscillation shown as Fig. 8(e), they calculated the energy conversion during a bouncing process and found that more than 80% of the energy is dissipated in the air film shown as Fig. 8(f), which indicates the importance of the air film dissipation to the overall droplet bouncing dynamics [66,67].

3.3. Bouncing on heated surfaces

The aforementioned droplet bouncing happens at room temperature, in which the air film is found to be a fundamental factor for realizing non-wetting state and determining the droplet bouncing dynamics. For droplet impact at room temperature, the air film can be maintained by using hydrophobic surfaces or decreasing the impact velocity of droplet to <0.75 m/s (or $We < 4$). Another way to realize non-wetting state is to actively maintain vapor film between the droplet and surface by heating the surface far beyond the liquid saturation temperature [8,11]. The

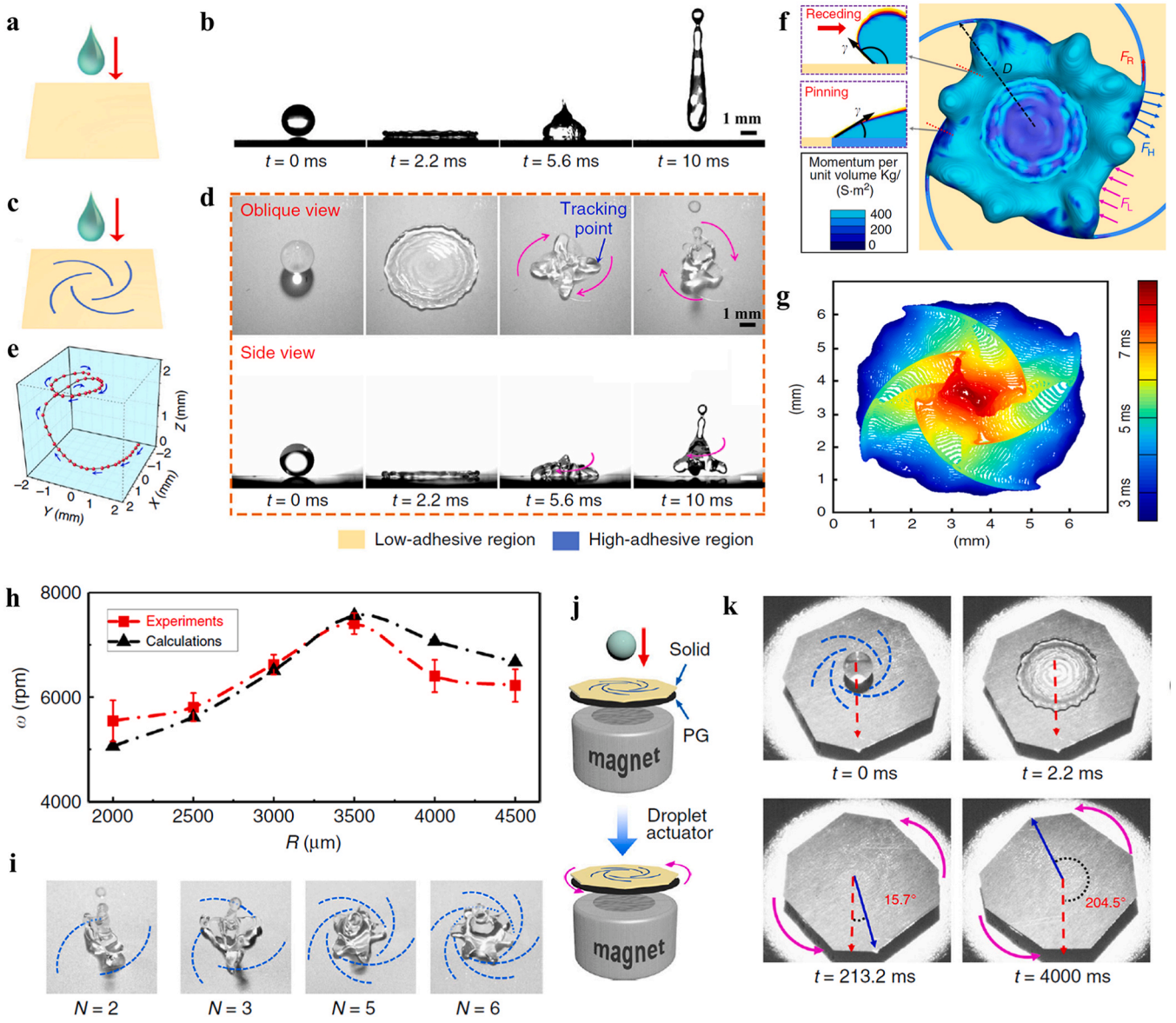

Fig. 7. Gyrating bouncing on surfaces with heterogeneous wettability [64]. (a), (b) Schematic and captured images of droplet impact on homogeneous hydrophobic surface. (c), (d) Schematic and captured images of droplet impact on hydrophobic surface with hydrophilic pattern. (e) Trajectory of the tracking point marked at $t = 5.6$ ms in (d). (f) Force analysis of the droplet receding on heterogeneous surface. The interaction of adhesive forces on hydrophobic region F_L and hydrophilic region F_H causes gyrating forces F_R. (g) Triple-phase contact line at various time reveals that the droplet motion on the hydrophobic region is much faster than that on hydrophilic region. (h) Relationship between instantaneous gyrating speed of the droplet and radius of the spiral R at We of 93. (i) Morphology of gyrating droplets on hydrophilic patterns with spiral number N of 2, 3, 5 and 6. (j), (k) Water droplet impact on a magnetically-levitated pyrolytic graphite (PG) flake with heterogeneous wettability at We of 93.

liquid at the droplet-surface contact area evaporates quickly to form continuous vapor film with thickness of ~100 μm beneath the droplet, which prevents the droplet from wetting the surface and leads to droplet bouncing [11]. In fact, droplet impact on heated surfaces is more common in industrial applications [16–20], such as spray cooling, fire extinguishing, direct fuel injection combustion and metal quenching.

Droplet bouncing on heated surfaces has been observed for a long time, while it was named after Johann Gotlob Leidenfrost in 1756 because he carefully conducted experiments to prove the existence of the vapor film between the droplet and heated surface [69]. Therefore, droplet bouncing on heated surface is well known as Leidenfrost phenomenon and the critical surface temperature for inducing such phenomenon is defined as Leidenfrost point [11,70]. In the past decades, the research of Leidenfrost phenomenon mainly focuses on two key aspects. One is the visualization of the vapor film, another is the manipulation of the Leidenfrost point. From these two aspects, the effect of droplet properties, surface characteristics and ambient conditions on the Leidenfrost phenomenon was widely investigated [8,11,71].

For the visualization of the vapor film, as mentioned in Section 2.4, high-speed video measurement technologies based on interference and reflection methods were applied to capture the vapor film geometry as well as to characterize the thickness of the vapor film [11,31–34,72,73]. The thickness of vapor film is assumed to be constant for small droplet with radius much smaller than the capillary length ($l_c = (\gamma/\rho g)^{1/2}$, where γ and ρ represent the surface tension and density of the droplet, and g represents the gravitational acceleration). However, such an assumption is not appropriate for lager droplet with radius comparable to or larger than the l_c. For droplet with radius larger than the l_c, the vapor film presents pocket geometry with film thickness decreases from the center to the edge [73], which was well proved by several experimental studies

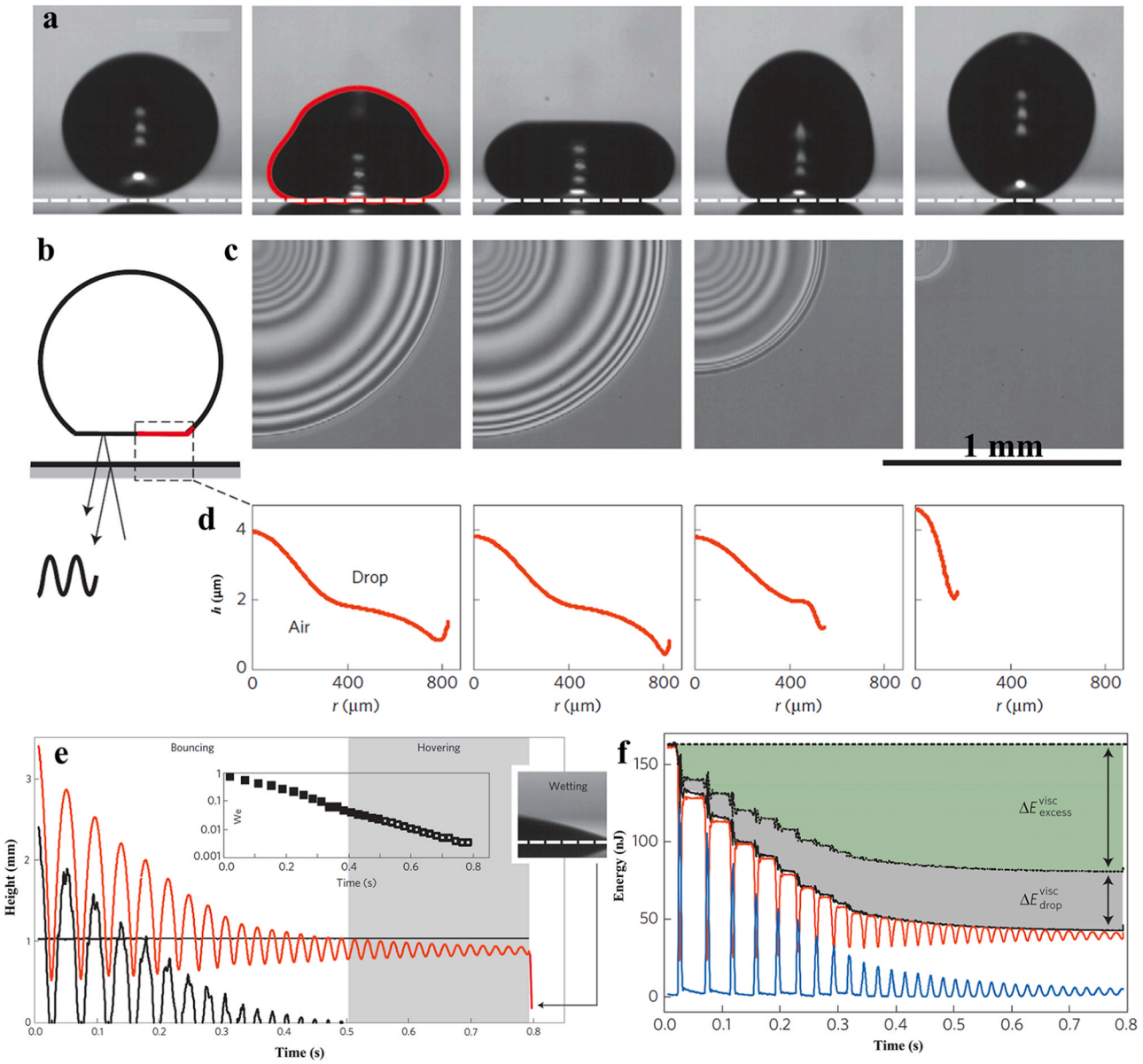

Fig. 8. Water droplet bouncing on hydrophilic glass substrate with equilibrium CA of 3° [66]. (a) Droplet impact process with impact velocity of 0.22 m/s. (b) Schematic diagram of the interference microscopy method. (c), (d) Interference patterns and thickness profiles of the air film beneath the droplet. (e) Time evolution of center-of-mass height of a water droplet with radius of 1.03 mm (red line) and minimum air height (black line) during the droplet impact on the smooth hydrophilic glass surface. The inset figure shows the inherent decrease of *We* during the experiment. (f) Energy conversion of the bouncing droplet shown in (a), where ΔE^{visc}_{drop} represents the viscous dissipation in the droplet and ΔE^{visc}_{excess} represents the viscous dissipation in the air film (For interpretation of the references to colour in this figure legend, the reader is referred to the web version of this article).

[31–34]. As shown in Fig. 9(a)–(c), Burton et al. directly observed the vapor pocket from the bottom view by using the interference method. They reconstructed the quantitative geometry of the Leidenfrost droplet with four different radius shown as Fig. 9(d), and the results show that flat bottom forms at small radius while vapor pocket forms at large radius. In addition, the thickness of the vapor pocket at center region was measured as 5–100 μm when increasing the droplet size shown as Fig. 9(e) [32].

For the manipulation of the Leidenfrost point, researchers have proposed numerous solutions to decrease or increase the Leidenfrost point by varying the impact velocity, surface tension, chemical component of the droplet [33,71,74,75], thermal conductivity, topography of the solid surface [76–83], and ambient conditions including gravity [84], vibration [85], electrical field [31] and pressure [86,87]. Among these parameters, the surface topography was found to affect the Leidenfrost point significantly. However, most of the reported surface topographies increase the Leidenfrost point [88–91], while only a few of surface topographies can decrease the Leidenfrost point [72,83]. In most of the industrial application, increasing the Leidenfrost point could enhance the heat transfer coefficient at high temperature condition and therefore improve the performance of industrial equipment [16–20]. However, low Leidenfrost point is more preferable for some special applications, such as biomedicine and droplet transportation [14].

In addition to the two issues mentioned above, researchers have also tried to control the droplet motion on heated surface by designing heterogeneous surface topographies and varying ambient conditions [88–94]. Among these studies, the directional movement of Leidenfrost droplet on heated surfaces was mostly concerned [88–90]. Agapov et al. designed surface with asymmetric, tilted nanopillars array to realize directional droplet motion on heated surface [88]. Zhang et al. and Li

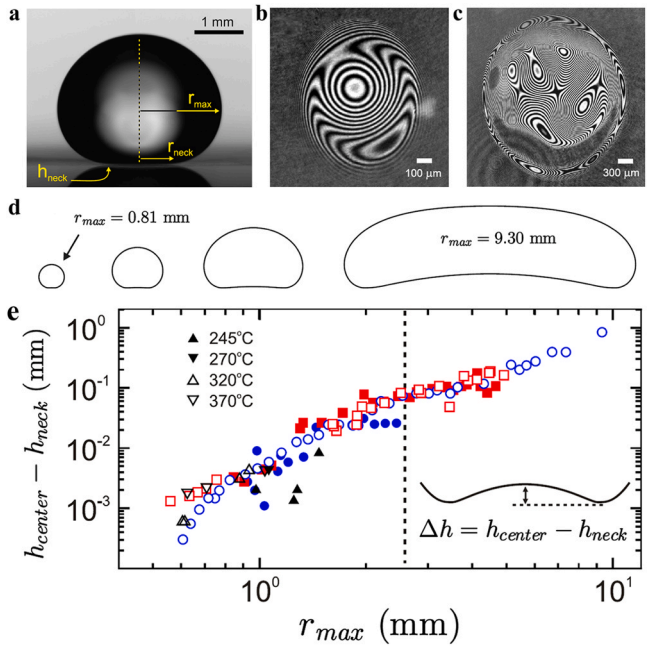

Fig. 9. Geometry and thickness profile of the vapor film beneath a Leidenfrost water droplet [32]. (a) Water Leidenfrost droplet on a substrate with surface temperature of 320 ℃, where r_{max} and r_{neck} represent the maximum droplet radius and neck radius, and h_{neck} represents the height of the neck to the surface. (b), (c) Interference patterns of Leidenfrost water droplet with maximum radius r_{max} of 1.2 mm and 2.7 mm. (d) Reconstruction of Leidenfrost water droplets with different radius. The vapor pocket becomes obvious for large size droplet. (e) Thickness of the vapor pocket at center region for Leidenfrost water droplets with different droplet radius on substrate with various surface temperatures.

et al. designed Janus-textured surfaces with patterned surface topography to break the wetting symmetry of a droplet, so as to realize self-propulsion of Leidenfrost droplets [89,90]. Fig. 10(a) shows the SEM images of Janus-textured surface with nanostructured/smooth silicon region that fabricated by Zhang et al., and Fig. 10(b) shows the droplet behaviors on the Janus-textured surface at different surface temperatures. At relatively low surface temperature (150 °C, 220 °C), the droplet tends to wet the nanostructured region, which shows the wettability difference of nanostructured/smooth regions. At surface temperature of ≥230 °C, the droplet presents contact-boiling at nanostructured region and presents film boiling at smooth region, as a result, the explosion of vapor bubbles forces the droplet to move towards the smooth region. At surface temperature of ≥320 °C, the droplet presents film boiling at both nanostructured/smooth regions, so the droplet bounces upward directly and no directional droplet motion happened [89]. Fig. 10(c) shows the gradient surface that fabricated by the Li et al., the surface zone with dense post distribution presents lower CA than that with sparse post distribution. Based on this concept, they designed Janus-textured surfaces that composed of four zones with different post density shown as Fig. 10(d) and (e). When the droplet impact on the heated Janus-textured surfaces, the number and size of the vapor bubbles increase as the post density increases, so pressure gradient forms at the Janus-textured surfaces to force the Leidenfrost droplet to move towards the zone with sparse post distribution at surface temperature of 270 °C [90].

Ambient pressure was also found to affect the Leidenfrost phenomenon significantly because the liquid saturation temperature decreases sharply with the ambient pressure decreases [91,92]. The Leidenfrost point of water droplet on a smooth surface at atmospheric pressure was reported as ~190 °C [16]. However, Celestini et al. found that the Leidenfrost point could be decreased to 33 °C when the ambient pressure is reduced to 50 mbar [93]. Orejon et al. carefully explored the effect of the ambient pressure on the Leidenfrost point and proposed a physical approach to predict the dependence of Leidenfrost point on ambient pressure [86]. Yu et al. explored the droplet behaviors on heated surface at ambient pressure of 0.2 kPa to 20 kPa and surface temperature of 20–200 °C with the experimental set up shown as Fig. 11(a), and the droplet behaviors under various conditions are listed in Fig. 11(b). Besides the evaporation, contact boiling and film boiling (Leidenfrost bouncing) phenomenon, an explosive bouncing phenomenon shown as pink lower triangle symbol was observed at ambient pressure of ≤6 kPa and surface temperature of 60–160 °C. The variation of explosive bouncing shown as Fig. 11(c) and Leidenfrost bouncing shown as Fig. 11(d) lies in the difference of vapor film dynamics. For the Leidenfrost bouncing, a continuous vapor film forms beneath the droplet to prevent the droplet from wetting the surface, so the droplet bounces like on the slippery super-hydrophobic surface. However, for the explosive bouncing, the droplet wets the surface initially due to the low ambient pressure, and local vapor bubble forms at the droplet-surface interfaces. The settled triple phase contact line provides an enclosed spacing for the pressure accumulation of local vapor bubble. Once the pressure of local vapor bubble exceeds a critical value, it explores dramatically and lifts up the droplet. They supposed that lowering the ambient pressure promotes the explosive bouncing in two aspects: (1) making the droplet easier to wet the surface at high surface temperature and thus leads to the formation of local vapor bubble; (2) lowering the critical explosion pressure of the local vapor bubble [94].

3.4. Bouncing on liquid film/bath

The splashing phenomenon of raindrops impact on liquid film/bath arouses the curiosity of countless observers. However, by taking a further observation of the droplet impacting process, some satellite droplets that generated from the splashing process would bounce or float on the liquid film/bath. Similar phenomena are widely observed in daily life and industry, such as stone erosion, sprinkling irrigation, spraying cooling, direct fuel injection and so on [6,9,17–20]. Therefore, the investigation of droplet impact on liquid film/bath could have a broad appeal to the development of numerous industrial technologies.

The liquid film and liquid bath are distinguished by the ratio of liquid depth to the droplet diameter (h/d_{drop}). If $h/d_{drop} < 1.5$, the liquid layer is assumed to be liquid film. If $h/d_{drop} > 1.5$, the liquid layer is assumed to be liquid bath [6]. Compared to droplet impact on solid surfaces, the droplet impact on liquid film/bath is more complicated because both the two liquid components and air/vapor film are subject to complex geometry deformation, energy transfer and internal flow [6,9]. Besides, the Van der Waals force between the two liquid components plays an importance role in determining the droplet bouncing dynamics. In general, droplet bouncing on liquid film/bath happens at low impact velocity (or low *We*), in which the air/vapor film was drain to a critical value at which the Van der Waals force between the two liquid components become unimportant. If the thickness of air/vapor film is smaller than the critical value, the air/vapor film collapses due to the cohesive Van der Waals force acting between the two liquid components and thereby coalescence happens. The critical thickness of air/vapor film is typically on the order of ~100 nm [95], depending on the liquid/air/vapor properties and system cleanliness.

Liquid film cannot exist solely, so the study of droplet impact on liquid film usually refers to the droplet impact on solid surface with a thin layer of another liquid [9]. Because the liquid film is soft and mobile, the droplet may penetrate the liquid film easily. If the droplet and liquid film are composed of two miscible liquids, the droplet is easy to merge with the liquid film. Therefore, it is difficult for droplet to bounce on horizontal surfaces with another miscible liquid film. Instead, previous studies mainly focus on the droplet bouncing on inclined surfaces or horizontal surfaces with another immiscible liquid film [96–99]. Moreover, there exist an upper limit and a lower limit for the critical *We*

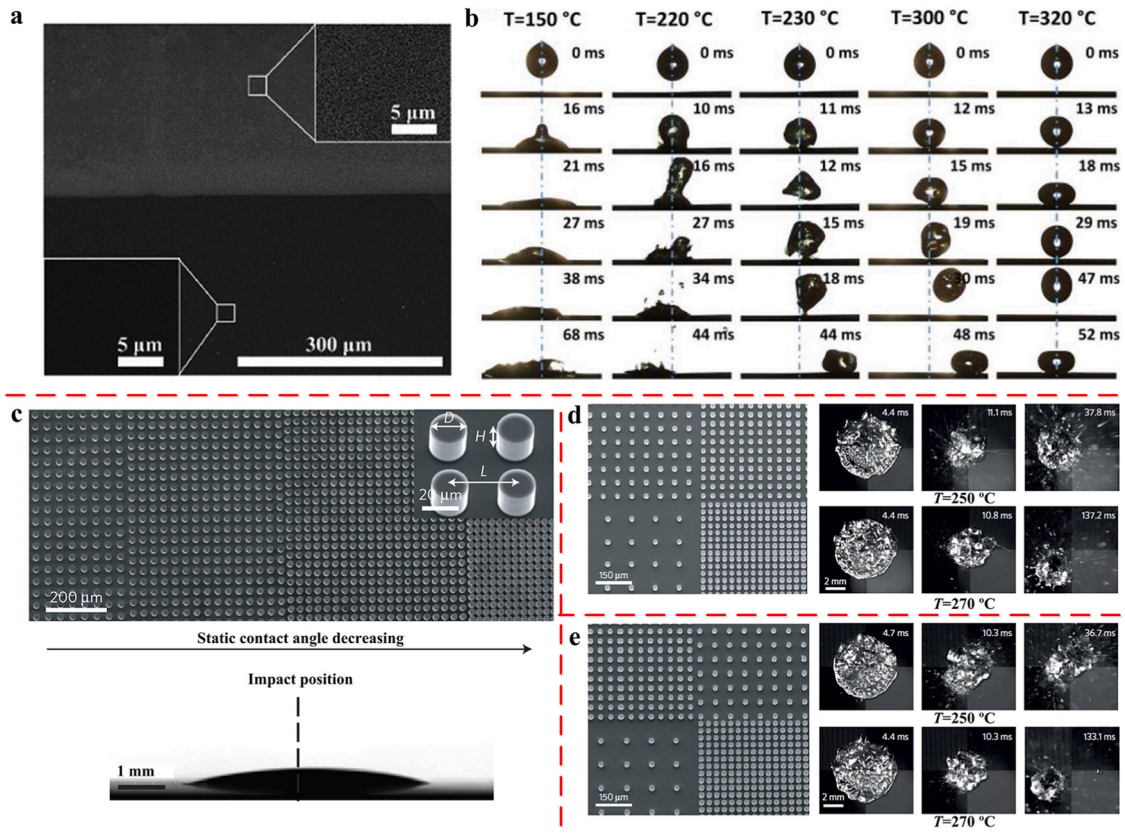

Fig. 10. Self-propulsion of water droplets on Janus-textured heated surfaces [89,90]. (a)–(d) Morphology of Janus-textured substrate with (a) nanostructured silicon substrate (top side)-smooth silicon substrate (down side). (b) Water droplet behaviors on Janus-textured with NSis-SSis structure at different surface temperatures. (c) Morphology and wettability of gradient surface with post spacing L of 25–105 μm at step increment of 5 μm. (d) (e) Directional moving of droplets on two Janus-textured surfaces with four different zones at surface temperature of 250 °C and 270 °C. The droplets move towards the zone with sparse post distribution at surface temperature of 270 °C.

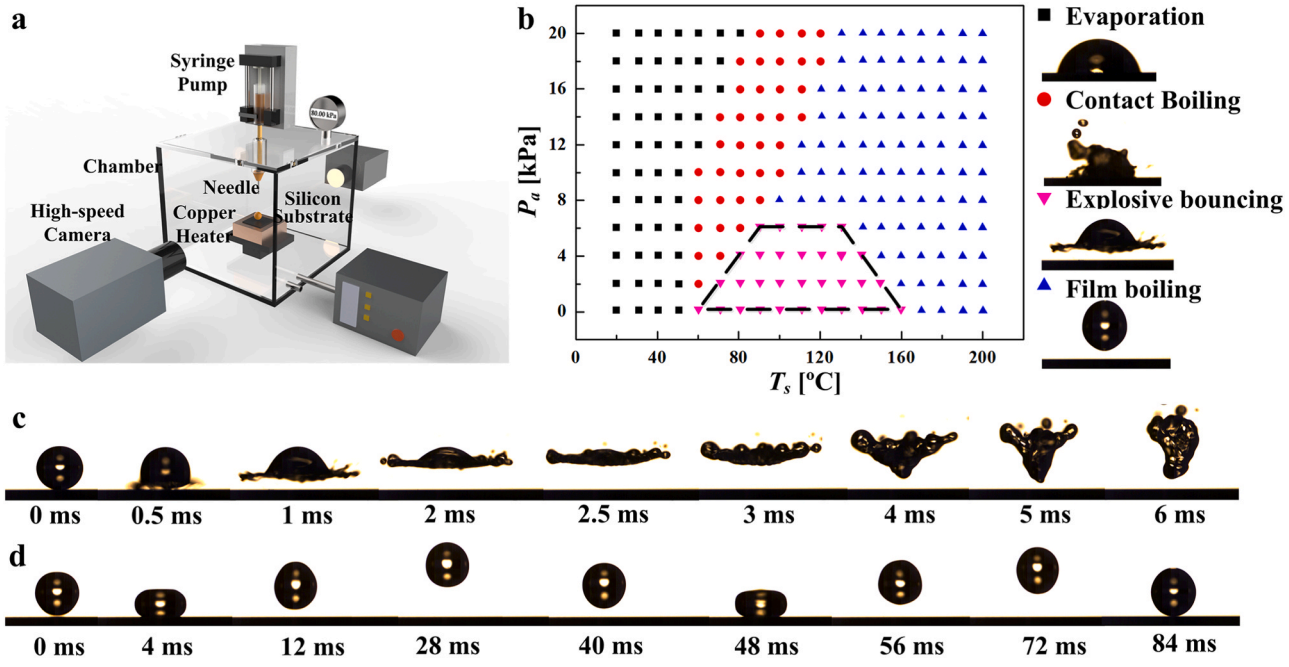

Fig. 11. Explosive bouncing [94]. (a) Schematic of the experimental setup. (b) Phase diagram of the droplet behaviors at various ambient pressure P_a and surface temperature T_s. (c) Explosive bouncing at P_a of 4 kPa and T_s of 110 °C. (d) Leidenfrost bouncing at P_a of 12 kPa and T_s of 130 °C.

for droplet bouncing on liquid film [9]. For *We* above the upper limit, the air/vapor film between the liquid film and droplet is damaged by the high shear force upon impact, so the droplet penetrates the liquid film and splashing happens. For *We* below the lower limit, the air/vapor has enough time to drain out, the droplet contacts with the liquid film and its kinetic energy is dissipated quickly, so the droplet may not gain enough kinetic energy to bounce off the wetted surface. The specific values of the upper and lower limits of critical *We* depend on numerous parameters, such as chemical component of the two liquids, surface curvature and surface orientation [9]. Hao et al. reported a super-hydrophobic-like water droplet bouncing on wetted flat surface with another immiscible liquid film, and they found that the percentage of droplet bouncing is 75–90% if $We < 10$ and drops sharply to zero if $We > 18$ [97]. Liang et al. founded that the upper *We* for butanol droplet bouncing on butanol-wetted cylinders keeps constant as ~9.2 if the curvature of cylinder is <0.5 and decreases if the curvature of cylinder is >0.5 [99].

Similar to the droplet impact on liquid film, the droplet also tends to merge with the liquid bath in most instances. However, such merger can be eliminated by intervening air/vapor film that exerts a lubrication force to overcome the gravity and Van der Waals force. There are some methods for realizing such intervening air/vapor film, including relative motion between the droplet and the liquid bath [100], heating the liquids and vibrating the liquid bath [101–105]. Among these methods, the droplet bouncing on vertically vibrated liquid bath was mostly concerned.

Droplet impact on vertically vibrated liquid bath can undergo coalescence, bouncing and walking, depending on the interplay of vertical acceleration of liquid bath δ, bouncing threshold δ_B and Faraday threshold δ_F. If $\delta < \delta_B$, the intervening air/vapor film fails to maintain the critical thickness and thus coalescence takes place. If $\delta > \delta_B$, the air/vapor film is sustainable to prevent coalescence and enable periodically and indefinitely droplet bouncing behaviors. If $\delta > \delta_F$, the bouncing droplets may begin to walk on the liquid bath, which is well known as walkers. The walkers only happen at limited conditions, and moving speed of the droplet is an important index for evaluating the walkers. In the commonly studied system, walkers are typically driven by a pure sine wave, and the maximum moving speed of a silicone oil droplet with radius of 0.3–0.5 mm is 15 mm/s shown as Fig. 12(a). Recently, Valani et al. present a new droplet walking phenomenon, which they called superwalkers, by using two waves with driving frequency of f and $f/2$ and phase difference of $\Delta\phi$ shown as Fig. 12 (b). With such a system, superwalkers in Fig. 12(c) with radius up to 1.4 mm can be speed up to 50 mm/s, which is the largest walker and maximum speed reported in the literature [102]. Detailed reviews about experimental observation and theoretical modeling of droplet impact on vertically vibrated liquid bath are provided by Bush and his co-workers [104,105].

3.5. Bouncing on liquid droplet

Collision of two miscible liquid droplets commonly leads to uncontrolled coalescence, while bouncing was only observed at very limited conditions [106–117]. In the bouncing regime, the inertial energy of the colliding droplets should be totally converted into droplet surface energy or consumed by viscous dissipation before the thickness of the air film between the droplets reduces to a critical value. The relative impact velocity of the two droplets is the key factor for influencing the thickness of air/vapor film, and bouncing mainly happens at moderate relative impact velocity [106–117]. For low relative impact velocity, coalescence happens because there is enough time for the air/vapor between the droplets to drain out. For high relative impact velocity, coalescence also happens because the air/vapor film is broken by the large inertial force of the colliding droplets.

In early studies, bouncing of two equal-sized water droplets was only observed for near grazing collision, in which stable air/vapor film is easier to form due to the small inertial force [106–109]. However, in recent decades, researchers have observed bouncing of two head-on droplet collision in which one droplet impacts on the top of another droplet from a certain height [110–115]. By taking a further consideration of the air/vapor film between the droplets, several methods were proposed to extend or reduce the bouncing regime of colliding droplets, including controlling surface tension gradient of the droplets [111,112], using electric field [113,116] and applying thermo-capillary [114,117]. Cira et al. mixed propylene glycol and water with various concentration to form two-component droplets with different surface tension, and they found that the high PG concentration droplet bounce spontaneously on the low PG concentration droplet shown as Fig. 13(a) and coalescence happens when the surface tension of the two droplets is similar shown as Fig. 13(b). They demonstrated that the evaporation rate difference of the two liquid component forms a thin vapor film to prevent the droplets from coalescing [111]. Ristenpart et al. observed bouncing phenomenon of two oppositely charged droplets by applied an electric field with a potential difference of 1 kV over approximately 1 cm shown as Fig. 13 (c). Different from the conventional indefinitely droplet bouncing, droplet bouncing occurs inevitably if a proper electric field is applied [113]. Yi et al. found the droplet bouncing is indefinitely even under fixed conditions and the bouncing possibility of droplets decreases with the droplet's temperature. They demonstrated that it is the water vapor around the heated droplets breaks of the air film and induces droplet

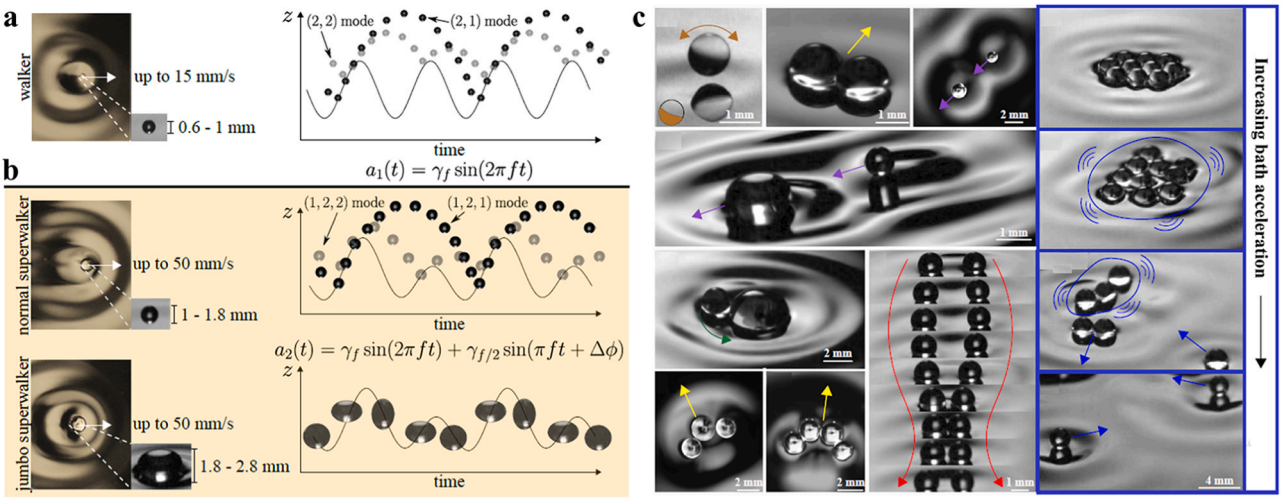

Fig. 12. Superwalkers [102]. (a) Walker driven by a single sine wave. (b) Comparison of normal superwalker and jumbo superwalker driven by two sine waves at frequencies of f and $f/2$ with phase difference of $\Delta\phi$. (c) Numerous phenomena of superwalkers observed by Valani et al.

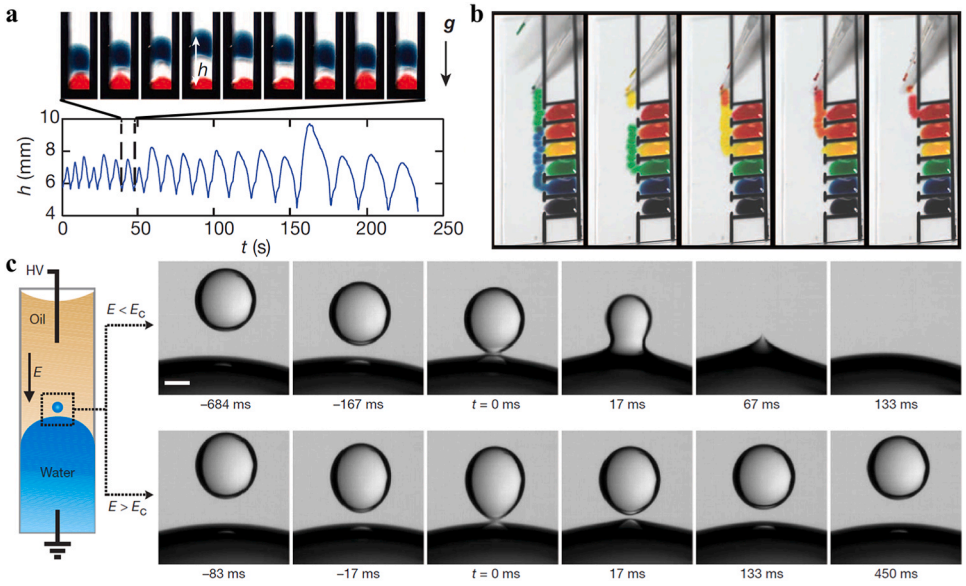

Fig. 13. Droplet bouncing on another droplet [111,113]. (a) Droplet with 25% propylene glycol (PG, blue) bounces on droplet with 1% PG (red). (b) Droplet sorting between 30% PG droplets (red) and 5% PG droplets (blue). (c) Coalescence and bouncing of two charged droplet. For low electrical field strengths of $E < E_c$, the droplets coalesce. For high electrical field strengths of $E > E_c$, the droplets separate from each other (For interpretation of the references to colour in this figure legend, the reader is referred to the web version of this article).

coalescence [114].

In addition to the vertical head-on droplet collision, horizontal head-on droplet collision on super-hydrophobic surfaces is a fundamental issue in nature and many industrial applications. There are two bouncing dynamics lie in the horizontal head-on droplet collision. One is the two droplets separate and change move direction after collision, another is the two droplets bounce off the surface after coalescence (also known as coalescence-induced bouncing). The bouncing mechanism of the former one is similar to that of vertical head-on droplet collision, where a thin air/vapor film forms between the droplets to prevent the droplets from coalescing [118,119]. Compared with the vertical head-on droplet collision, the bouncing and coalescence of horizontal head-on droplet collision are easier to control on the super-hydrophobic surfaces [118,119]. Mertaniemi et al. investigated effect of *We* and collision parameters on the bouncing and coalescence of two horizontal head-on collision droplets on super-hydrophobic surfaces, and they found that the droplet bouncing or coalescence can be easily controlled by selecting proper *We* and collision parameters [118].

However, for the coalescence-induced bouncing, the droplets coalesce initially and bounce off the surface afterwards because part of the excess droplet surface energy is converted into upward kinetic energy. It is reported that the coalescence-induced bouncing only happens for tiny droplets with radius much smaller than the capillary length in which the gravity and viscous dissipation of the droplets can be ignored [120–123]. Vahabi et al. fabricated superomniphobic surfaces with a macrotexture to realize coalescence-induced bouncing. The macrotexture redirects the in-plane velocity vectors to out-plane velocity vectors, so the energy conversion efficiency (ratio of upward kinetic energy to the excess surface energy of droplets) reaches up to 18.8%, which is about 570% enhancement compared to superomniphobic surfaces without a macrotexture [120]. Miljkovic et al. found that the coalescence-induced bouncing droplet gains a net positive charge when it departs from the solid surface. Based on this finding, they applied electric field with negative/positive voltages to enhance/weaken the droplet bouncing [122].

4. Potential applications

After comprehensive understanding of the water droplet bouncing phenomena and mechanisms, numerous advanced droplet bouncing-based applications were developed, such as surface self-cleaning, anti-smudge, anti-fouling, deicing, directional droplet transportation and heat transfer enhancement. Besides, some special applications based on the droplet bouncing were also developed, such as droplet logic gate and electrical generation.

4.1. Surface self-cleaning

Surface self-cleaning technology has attracted extensive attention over the past century due to its widely application from windows glasses to solar cell panels [1–3]. Inspired by many natural self-cleaning surfaces, such as lotus leaf, rice leaf, butterfly wing, cicada wing, snail shell and shark skin, super-hydrophobic and super-hydrophilic surface processing technologies were developed to realize self-cleaning surfaces [3]. For the super-hydrophilic surfaces, the water wets the surface texture and brings the contaminant away. However, the surfaces may keep wetted for a long time, which is undesirable in many applications. Compared to the super-hydrophilic surfaces, the water rolls off the super-hydrophobic surfaces and takes the contaminant away, which were confirmed to have high self-cleaning efficiency than that of super-hydrophilic surfaces [3]. The research on self-cleaning technology also promotes the development of numerous related surface technologies [3,124,125], such as anti-fogging, anti-smudge, anti-fouling, deicing, self-sterilizing, anisotropic wetting and directional adhesion.

Although the surface wettability mainly depends on the surface energy and topography of the solid surfaces, manipulating the droplet bouncing dynamics is reported to be another effective method for enhancing the self-cleaning efficiency of surfaces by reducing the droplet contact time, increasing droplet moving speed and preventing droplet from pinning on the surfaces. Through vast experimental and theoretical studies, several methods were proposed to settle these issues, such as breaking the symmetry spreading and receding of the bouncing droplet, regulating the surface orientation, lowering the ambient pressure and agitating the surrounding air [3,125]. As shown in Fig. 14(a)–(c), Schutzius et al. observed freezing induced droplet bouncing phenomenon on super-hydrophobic surfaces at low ambient pressure and low humidity condition, which might have broad application in surface deicing. Fig. 14(d) shows the thermographic image of the droplet shown in Fig. 14(c) from side and top views. It indicates that the high evaporation rate of the droplet at low ambient pressure results in droplet freezing at supercooled state, which induces a sudden increase in droplet evaporation and provides enough pressure to levitate the droplet [65]. More detailed researches about droplet bouncing on solid surfaces have been introduced in Sections 3.1–3.3.

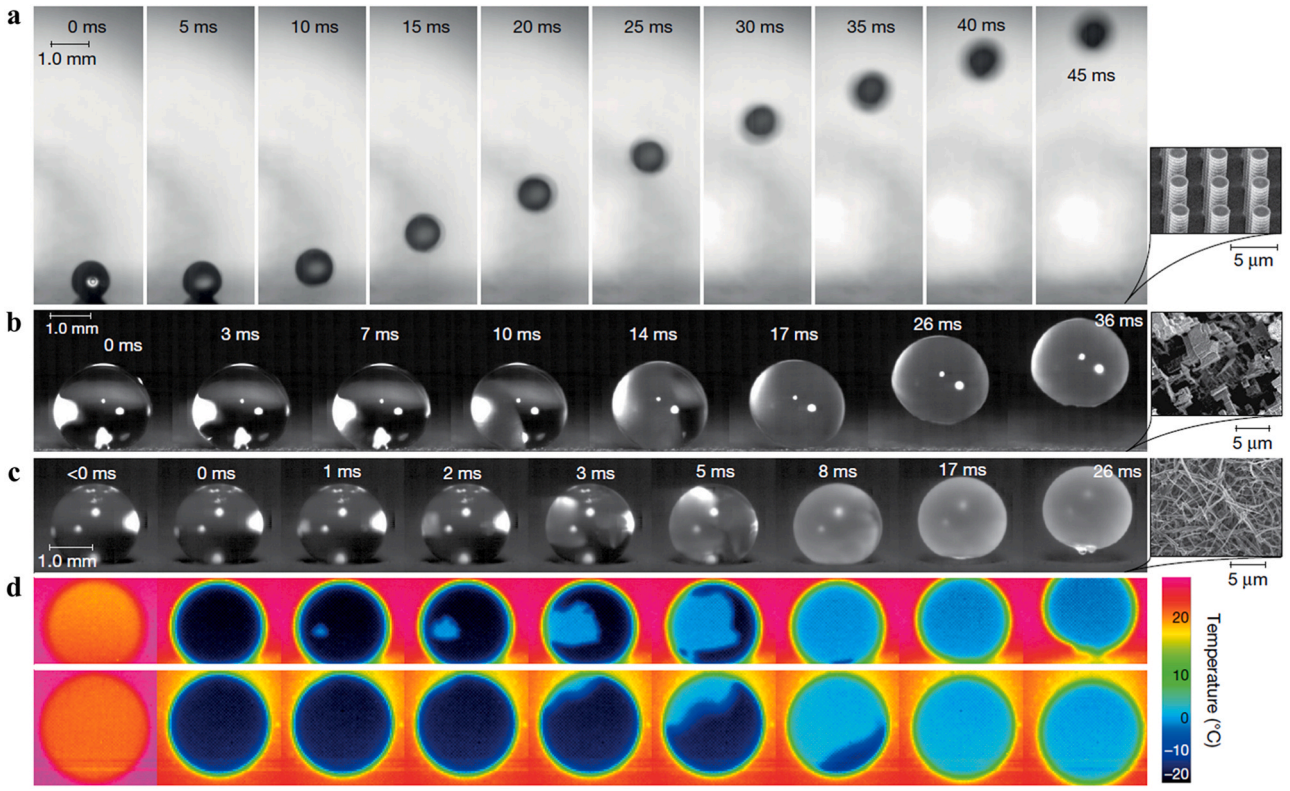

Fig. 14. Freezing induced droplet bouncing on super-hydrophobic surface at room temperature at low ambient pressure and low moisture condition [65]. (a) Silicon surface with micropillar array with diameter, spacing and height of 2.0, 4.6 and 13.5 μm. (b) Etched aluminum surface. (c) Surface with fluoropolymer–carbon-nanofibre composite. (d) Thermographic image of the droplet shown in (c) from side and top views.

Despite the self-cleaning technologies has been developed for over 100 years, it still faces many challenges. One of the challenges is the mechanical and chemical durability of the surfaces. The nano/micro surface topographies may be easily damaged by the external mechanical force and thermal stress, and oxidation happens when the metal surfaces are immersed in moisture and acid-alkaline-base environment, which causes unpredictable change to the surface wettability [3]. Compared to the super-hydrophobic surfaces, the super-hydrophilic surfaces are smoother and have better mechanical durability. However, the hydrophilic function groups on the surfaces present extremely low chemical and thermal durability, which hinders the commercial applications of super-hydrophilic surfaces [3]. With the development of surface processing technologies, some robust super-hydrophobic surfaces can be realized [23,28,30]. However, the cost of the surface topography construction process still discourages entrepreneurs and consumers. Last but not the least, the complexity of the contaminant may be one of the challenges for the self-cleaning technologies. In most of the previous studies, the contaminant is considered as powders. However, the contaminant could be any tiny liquid and solid particles. In fact, oil mist is a very common contaminant in practical applications. The low surface tension oil shows high adhesion on most of the super-hydrophobic surfaces, except for some well-designed superomniphobic surfaces [23,28]. Therefore, the oil mist is very difficult to be washed away and the accumulation of oil mist will deteriorate the self-cleaning ability of the surfaces.

4.2. Directional droplet transportation

Transporting liquid droplets in a target direction is a fundamental issue in numerous biological and chemical applications [13,14], such as microfluidics, combinatorial chemistry, and thermal/biomedical devices. Early droplet transport systems generate liquid droplets by a shear flow with another immiscible liquid and transport the generated droplets by another encapsulating liquid stream [14]. More recently, transporting liquid droplets by creating surface tension gradients within the droplet has made it possible to transport individual droplets without micro-channels and encapsulating liquids [14]. Several methods were proposed to create the surface tension gradient in droplet by modifying the wettability, topography, temperature and curvature of the surfaces, such as electrowetting, chemical gradient, anisotropic ratchet and titled pillars, and the droplet bouncing dynamics on these surfaces were carefully characterized by many researchers [14,88,126,127].

The anisotropic surface topographies, including anisotropic ratchet and tilted pillars, control the contact line pinning of the droplet to form a net force to move the droplet [14]. However, the transport distance of droplet on surfaces with solely anisotropic surface topographies is very limited, typically several millimeters, which is not enough for most practical applications [128–130]. To further increase the transport distance, researchers combined the wettability gradient with the thermal gradient by heating the surfaces with micro-ratchet-like crenellations above the Leidenfrost point [131–140]. As shown in Fig. 15(a), the flow of vapor below the droplet is rectified in the direction of descending slopes along the teeth of the ratchet due to the asymmetric geometry of the teeth, which generates viscous stress to force the Leidenfrost droplet to bounce and move in the desired direction shown as Fig. 15(b). By controlling the parameters of the ratchet, the moving speed of the droplet can be larger than 10 cm/s, which shows the superiority of ratchet in transporting droplet [132]. Recently, Feng et al. fabricated surfaces planted with sabina chinensis-like asymmetric tilted pillars to realize global transport of droplets. As shown in Fig. 15(c)–(f), water droplet sits at the tip of the pillar and gets ejected when it asymmetrically coalesces with neighboring droplets, the droplet gets kinetic energy from each coalescence and continuous to move with velocity of ~10 cm/s [141].

Electrowetting on dielectric is one of the best-developed method for directional droplet transportation [142–145]. It applies voltages at

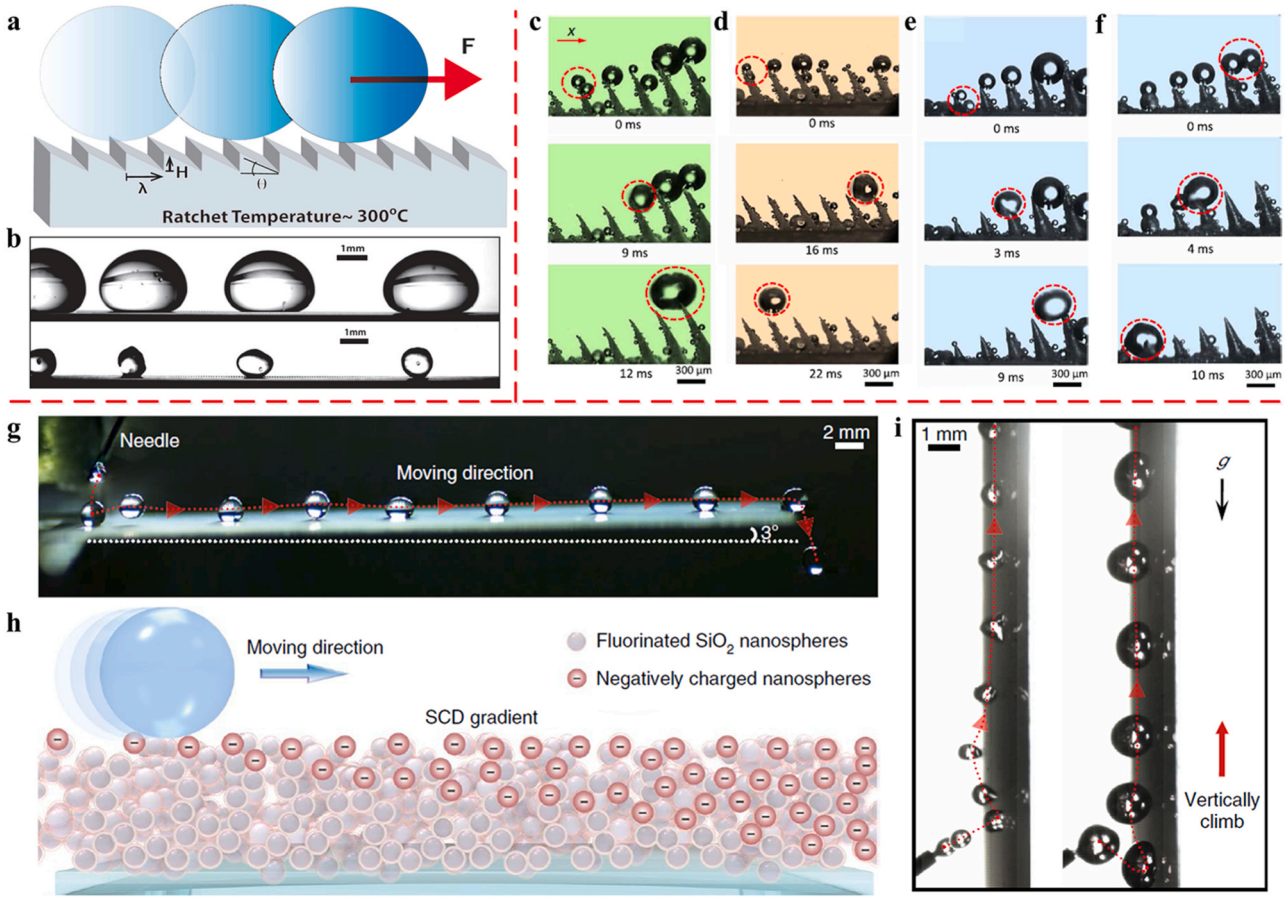

Fig. 15. Long distance droplet transportation. (a)–(b) Transportation of Leidenfrost water droplet on micro-ratchet [132]. (c)–(f) Droplet transportation on (c) pine needle–inspired asymmetric surface (PNAS), (d) Equally high Janus pillars surface and (e)–(f) conical needles [141]. (g)–(i) Droplet transportation on charged superamphiphobic surfaces with surface charge density gradient [144].

electrodes below the surface to induce a local reduction of surface tension at solid-liquid interface. The CA of droplet on the charged region reduces while it keeps constant on the uncharged region, which pulls the droplet to flow from uncharged region to charged region [142–145]. Sun et al. realized high velocity and ultralong distance droplet transportation by designing proper surface charge density gradients on superamphiphobic surfaces [144]. As shown in Fig. 15(g)–(i), the droplets exhibit a spontaneous, directional motion on the charged surfaces even the surface is vertically placed. By regulating the surface charge density gradient, they reported a maximum transport velocity of ~1.1 m/s, which might be the highest droplet transport velocity been reported in the literature.

4.3. Heat transfer enhancement

Most industrial applications involve droplet impact on heated surfaces [8,11,16–20], such as spraying cooling, metal quenching, fire extinguishing and direct fuel injection combustion. In these applications, the droplets impact on the heated surface and experience various behaviors from evaporation, contact boiling to film boiling (Leidenfrost phenomenon). The heat transfer coefficient between the liquid and surface is highly related to the droplet behaviors [8,20]. In general, contact boiling with fast evaporation rate is desirable for most applications, while film boiling with low evaporation rate should be suppressed [8,11,17–19]. An effective approach to suppress film boiling is to increase the Leidenfrost point by regulating the liquid properties, surface characteristics and ambient conditions, which was introduced in Section 3.3.

Another important droplet bouncing issue involved in heat transfer application is the droplet removal. The vapor condensates on the cooled surfaces and forms nano-/micro-droplet initially. If these droplets are not removed immediately, they form liquid film on the cooled surfaces, which reduces the heat transfer coefficient significantly. Therefore, it is very important to remove the pinning droplets from the surface in time. It is reported that designing surface topography to induce desirable coalescence-induced bouncing could be a preferable solution. Mukherjee et al. explored the effect of surface orientation on the coalescence and bouncing of condensed droplets, and they found that the condensed droplets is easier to coalesce and bounce on inclined surfaces due to the synergistically function of capillary-inertial and gravitational effects. As a result, the maximum droplet size on the inclined surfaces was an order of magnitude smaller than that on the horizontal surfaces, which enhance the theoretical heat transfer coefficient by 40% and 100% for the 45° tilt and vertical orientated surfaces [121].

4.4. Droplet logic gate

Combining microfluidic devices to realize complex “Lab-on-chip” systems has revolutionized the current healthcare diagnosis [146]. The fluid components, containing chemical, biochemical or biologic information, perform basic logical operations in the microfluidic devices, including AND/OR, NOT, NAND, ON/OFF, XOR/AND, XOR/NAND logic gates and flip-flop memory [12]. Although the fluidic logic gates cannot compete with solid logic gates in terms of processing speed, parallelism and power consume, they offer a feasible way to realize autonomous control in microfluidic devices and even perform calculations without resorting to external processing.

The usage of fluidic logic gates can be tracked back to the early 20th

century, when researchers tried to construct fluidic counterparts of digital electronics [12]. However, the potential of this method was widely known since Prakash et al. proposed "droplet logic operations" [147], which was further developed by Katsikis et al. in 2015 [148]. By introducing a rotating magnetic field to manipulate the motion of ferrofluid droplets, Katsikis et al. developed OR/AND, XOR/AND and XOR/NAND logic gates, memory loops, flip-flops and so on. There are more examples of droplet logic gates performed by Woodhouse and Dunkel [149], Cheow et al. [150], Vourdas et al. [151], and Zhou et al. [152], in which the logic gates were realized by control the motion of single droplet in micro-channel or another liquid stream.

Another method to realize logic gates is to manipulate the coalescence or bouncing behaviors of two collision-droplets [118,153,154]. The collision of two droplets in vertical direction commonly leads to indefinitely coalescence or bouncing, which blocks its application in industry. Therefore, researchers tried to find methods to control the coalescence or bouncing of two collision droplets. Draper et al. coated water droplets with super-hydrophobic powders to control the coalescence or bouncing of two collision droplets, so as to realize AND and AND-NOT droplet logic gates [154]. Mertaniemi et al. found a strategy to control bouncing or coalescence of two horizontal head-on collision droplets on super-hydrophobic surface by regulating the *We* and collision parameters. Based on this finding, they constructed NOT/FANOUT, AND/OR droplet logic gates and flip-flop memory [118]. For the NOT/FANOUT shown as Fig. 16(a)–(c), a droplet comes from the input 1 will leave through the output $\overline{A}$. However, if two droplets come from the inputs 1 and A at the same time, the collide and bounce of the two droplets at the cross point will result in both the two outputs A. Therefore, this droplet logic gate performs the logical NOT/FANOUT operation. For the AND/OR logic gate shown as Fig. 16(d)–(f), a droplet comes from the input A or B will leave through the output A+B. However, if two droplets come from A and B at the same time, the collide and bounce of the two droplets at the cross point will result in both the outputs A+B and A•B. Therefore, this droplet logic gate performs the logical AND/OR operation. For the flip-flop memory shown in Fig. 16 (g)–(i), a droplet sits at the middle of the device. If another droplet comes from the input, the two droplet collide and bounce at the middle of the device, the latter droplet pushes the former droplet to the outputs while it pins at the middle of the device. Therefore, it always keeps one droplet in the device, which could be defined as flip-flop memory.

4.5. Electrical generation

Energy crisis and global warming have become two serious problems over the world in 21st century, so developing clean energy technologies by utilizing renewable energy resources becomes extremely urgent. Water is a clean and renewable energy resource on earth. It contains abundant energy in the forms of chemical, thermal, kinetic and so on. The kinetic energy of water has long been utilized by large-scale hydropower, in which the dynamic flow of water stream is converted into electrical energy by the electro-magnetic generators. Although the hydropower can realize relatively high light conversion efficiency, it is most effective for high frequency water flow. However, plenty of water energies are stored in low frequency water flow in forms of raindrop, dew, tide and river/ocean wave, which are rarely exploited so far. In recent years, with the development of nanotechnology and nanoscale materials, new strategies towards harvesting energy from low frequency water flow based on hydrovoltaic effect and contact electrification were proposed. In the former method, the electrical energy generates from the direct interaction of carbon nanomaterials with flowing, waving, dropping and evaporating of water [155–158]. In the latter method, the electrical energy generates from the contact of charged water and thin dielectric layer through triboelectric nanogenerator (TENG) [159–162], droplet-based electricity generator (DEG) [163] and charge trapping-based electricity generator (CTEG) [164,165]. The TENG, first proposed by Wang's group in 2012, generates electrical energy based on the coupling of contact electrification and electrostatic induction [166,167]. So far, the TENGs have been applied to harvest energy from solid–solid [166,167], solid–liquid [159–161], liquid–liquid [168] and liquid/solid-air [169] interfaces. Among these applications, a TENG utilized at the solid–liquid interface can generate electrical energy from ocean/river waves [170] and droplets motion [171–179]. As shown in

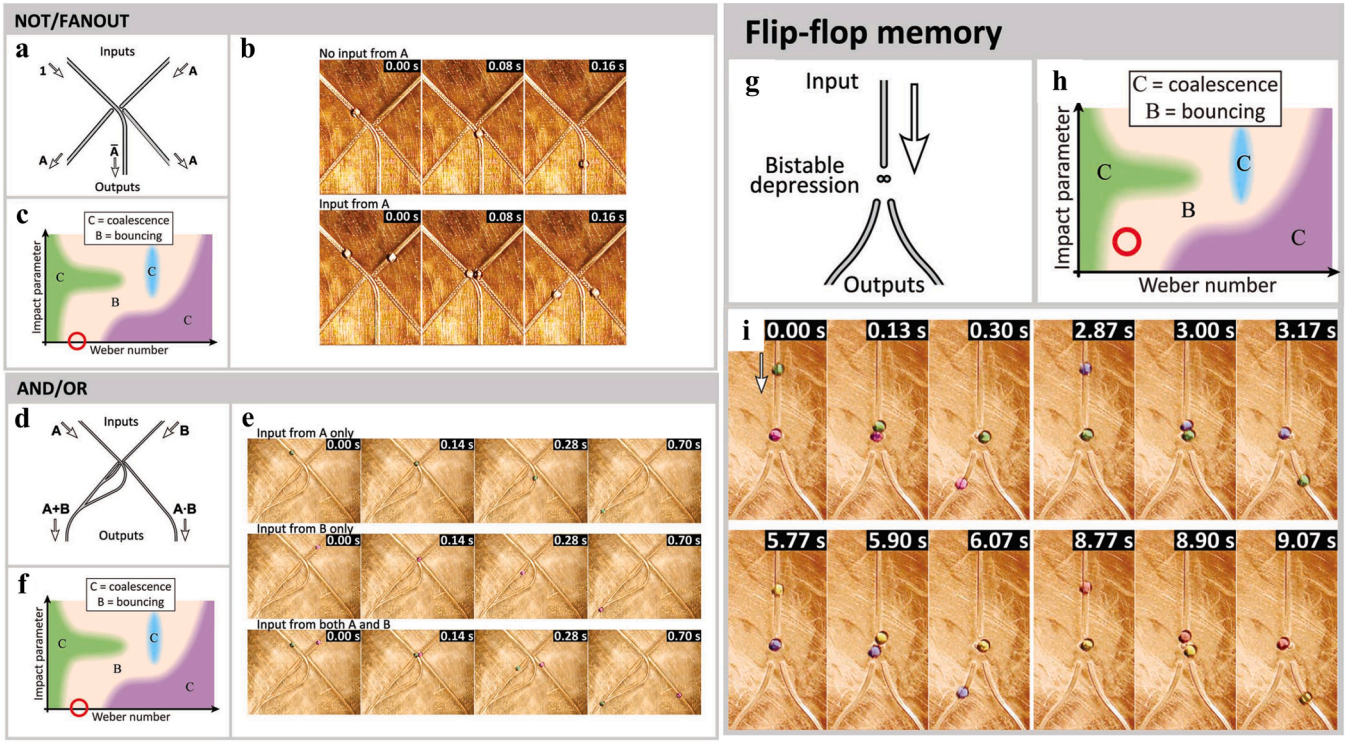

Fig. 16. Droplet logic gates and flip-flop memory [118]. (a)–(c) NOT/FANOUT, (d)–(f) AND/OR and (g)–(i) flip-flop memory.

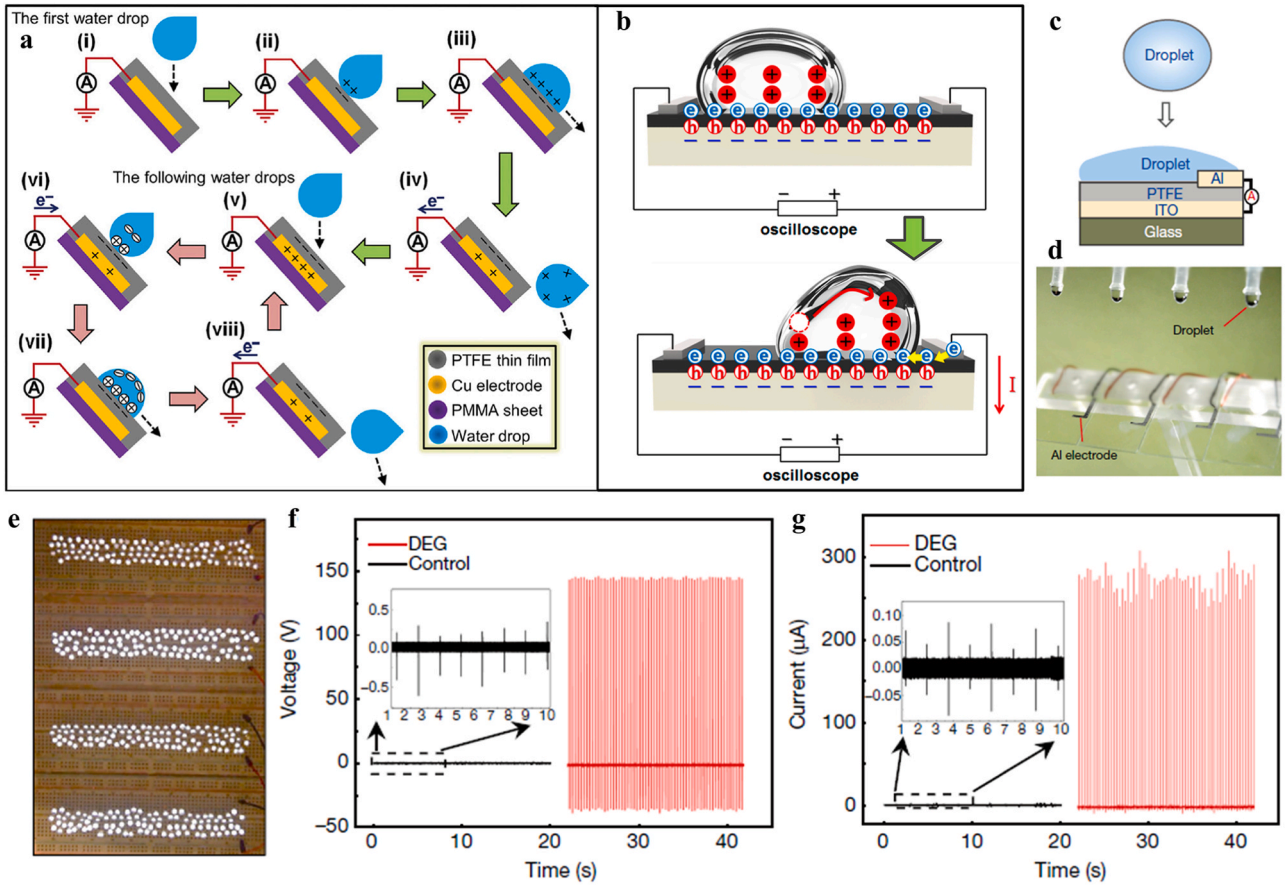

Fig. 17. Energy harvesting from droplets. (a) TENG with one electrode [159] and (b) with two electrodes [161]. (c)–(d) Schematic and experimental diagram of DEG device. (e)–(g) 400 LEDs is powered with open-circuit output voltage and short-circuit current of ~143.5 V and ~270 μA when four droplets of 100 μl release from a height of 15.0 cm to contact the DEG device [163].

Fig. 17(a) and (b), the TENGs used in droplet energy harvesting has one [159] or two [161] electrodes on a substrate that connected to an external electrical energy harvesting circuit. The electrodes are coated with hydrophobic or hydrophilic dielectric layer that carries some permanent surface charges [180–185]. When droplets impact the electrodes, it changes the capacitive coupling between the electrodes and generates electrical currents for energy harvesting from droplets (see the process i–viii in Fig. 17(a)). However, the low density and poor stability of the surface charges on dielectric layer causes extremely low droplet energy harvesting efficiency of traditional TENGs, typically ~0.01% [159]. Xu et al. developed a DEG to increase the droplet energy harvesting efficiency to ~2.2% [163]. As shown in Fig. 17(c) and (d), the impact water droplet spreads on the device and bridges the disconnected electrical components into a closed-loop circuit. Compared to the conventional TENG, the droplet in DEG not only provides the mechanical energy, but also contributes to the trapped surface charge generation on the polytetrafluoroethylene (PTFE). As a result, the DEG transforms the interfacial effect into bulk effect and increases the droplet energy harvesting efficiency by several orders of magnitude over the conventional TENGs. As shown in Fig. 17(e)–(g), 400 light-emitting diodes (LEDs) were instantaneously powered up when four droplets of 100 μl were released from a height of 15.0 cm to contact the DEG device, and the open-circuit output voltage and short-circuit current were measured as ~143.5 V and ~270 μA. However, the density and stability of the surface charges in the DEG is still at a low level, which blocks the upper limit of the droplet energy harvesting efficiency. To solve this issue, Wu et al. proposed a CTEG with pre-charged hydrophobic fluoropolymer films to further enhance the droplet energy harvesting efficiency to >11% [164,165]. They developed a homogeneous electrowetting-assisted charge injection (h-EWCI) method to pre-charge the electrodes. Therefore, the CTEG does not rely on the contact electrification upon drop impact and solves the instability of surface charges that exist in TENGs and DEGs. There are two recent review papers can be referred on the energy harvesting from droplet/liquid energy by Tang et al. in 2019 [186] and Wang et al. in 2020 [187].

5. Conclusions and perspectives

The droplet bouncing on surfaces has attracted extensive attention in recent decades not only because of its widely applications in daily life and industry, such as self-cleaning, anti-smudge, anti-wetting, spraying cooling, inject printing, internal combustion engine and metal quenching, but also due to its potential application in some emerging research fields, such as droplet transportation, liquid logic gates and water energy harvesting. This review presents an overview of recent progresses about droplet bouncing dynamics on hydrophobic/hydrophilic/heated surfaces and liquid film/bath/droplet. The underlying physics of droplet bouncing, such as rapid droplet impact dynamics, droplet-surface interaction, air/vapor film visualization, surface wettability/topography, was reviewed from the aspects of liquid properties, surface characteristics and ambient conditions. The absence of liquid/surface contact is proved to be the key factor for determining droplet bouncing dynamics, which can be achieved by lowering the *We* of droplet and designing hydrophobic surfaces, or actively maintaining the air/vapor film by heating the solid surface above the Leidenfrost point, vibrating the liquid bath, applying electric/magnetic/pressure fields and so on. Finally, some advanced applications based on droplet bouncing mechanism were introduced in this review, including surface self-cleaning,

directional droplet transportation, heat transfer enhancement, droplet logic gate and electrical generation.

Although significant progress has been made towards the droplet bouncing dynamics over the past decades, there are still many unsolved issues and substantial challenges in future development and applications.

(1) Experiment is the mainstream method to study the droplet bouncing dynamics so far, while reliable numerical modeling of droplet bouncing is still lacking. Numerical modeling of single droplet on a dry surface is much reliable at present, although argument lies in the boundary conditions definition of moving triple phase contact line and dynamic CA. However, numerical modeling of single/multiple droplets on wet/heated surface and liquid droplet/film/bath is still incompletely developed. In addition to triple phase contact line and CA, the definition of air/vapor deformation might be another significant obstacle lies in numerical modeling of droplet bouncing.
(2) Most of the experimental droplets are pure/deionized water without considering the impurity, salinity, pH and corrosively of water. In addition, droplet bouncing dynamics of other typical liquids, such as oil, ink, refrigerant and alcohols, that are widely applied in industrial applications was rarely concerned. Taking the above factors into consideration is of great significance to further explore the droplet bouncing mechanism and is helpful for promoting the droplet-based applications.
(3) The diameter of experimental droplets is basically on the order of millimeter, while micro/nanometer droplets are more common in practical applications. Experimental investigation and numerical modeling of micro/nanometer droplets impact on the surfaces could have more broad appeal to the development of industrial technologies.
(4) Air/vapor film is proved to be a fundamental issue in determining the droplet bouncing dynamics. However, directly observation of air/vapor film is partially achieved on smooth and transparent surfaces, which is far from the practical condition. Therefore, it is very important to develop novel high-speed video measurement technology to observe and characterize the air/vapor film profile on rough/opaque surfaces as well as on liquid droplet/film/bath.
(5) Most of the existing surface processing technologies for constructing micro/nanoscale surface topographies are complex, expensive and time-consuming. Moreover, the stability of the surface topography under mechanical force and chemical contamination is always a considerable challenge for surface design. Considering the importance of surface characteristics for determining droplet bouncing dynamics, it is urgent to develop simple, efficient and costless approaches to construct robust and durable micro/nanoscale surface topographies.

Declaration of Competing Interest

The authors declare that they have no known competing financial interests or personal relationships that could have appeared to influence the work reported in this paper.

Acknowledgments

This work is supported by the National Natural Science Foundation of China (51625601, 52076087), the China Postdoctoral Science Foundation (2020M672346), the Ministry of Science and Technology of the People's Republic of China (2017YFE0100600), the financial support from Creative Research Groups Funding of Hubei Province (2018CFA001), the Open Project Program of Wuhan National Laboratory for Optoelectronics (2018WNLOKF017) and Postdoctoral Creative Research Funding of Hubei Province.

References

[1] B. Bhushan, Y.C. Jung, Natural and biomimetic artificial surfaces for superhydrophobicity, self-cleaning, low adhesion, and drag reduction, Prog. Mater. Sci. 56 (2011) 1–108.
[2] K. Koch, B. Bhushan, Y.C. Jung, W. Barthlott, Fabrication of artificial Lotus leaves and significance of hierarchical structure for superhydrophobicity and low adhesion, Soft Matter 5 (2009) 1386–1393.
[3] S. Nishimoto, B. Bhushan, Bioinspired self-cleaning surfaces with superhydrophobicity, superoleophobicity, and superhydrophilicity, RSC Adv. 3 (2013) 671–690.
[4] Y. Wang, K. Ma, J.H. Xin, Stimuli-responsive bioinspired materials for controllable liquid manipulation: principles, fabrication, and applications, Adv. Funct. Mater. 28 (2018) 1–28.
[5] L. Xu, W.W. Zhang, S.R. Nagel, Drop splashing on a dry smooth surface, Phys. Rev. Lett. 94 (2005) 1–4.
[6] C. Tropea, M. Marengo, Impact of drops on walls and films, Multiph. Sci. Technol. 11 (1999) 19–36.
[7] C. Josserand, S.T. Thoroddsen, Drop impact on a solid surface, Annu. Rev. Fluid Mech. 48 (2016) 365–391.
[8] G. Liang, I. Mudawar, Review of drop impact on heated walls, Int. J. Heat. Mass Transf. 106 (2017) 103–126.
[9] G. Liang, I. Mudawar, Review of mass and momentum interactions during drop impact on a liquid film, Int. J. Heat. Mass Transf. 101 (2016) 577–599.
[10] A.L. Yarin, Drop impact dynamics: splashing, spreading, receding, bouncing…, Annu. Rev. Fluid Mech. 38 (2006) 159–192.
[11] D. Quéré, Leidenfrost dynamics, Annu. Rev. Fluid Mech. 45 (2013) 197–215.
[12] J. Čejková, T. Banno, M.M. Hanczyc, F. Štěpánek, Droplets as liquid robots, Artif. Life 23 (2017) 528–549.
[13] A. Nakajima, Design of hydrophobic surfaces for liquid droplet control, NPG Asia Mater. 3 (2011) 49–56.
[14] H.R. Holmes, K.F. Böhringer, Transporting droplets through surface anisotropy, Microsyst. Nanoeng. 1 (2015) 1–9.
[15] M.R.O. Panão, A.L.N. Moreira, Flow characteristics of spray impingement in PFI injection systems, Exp. Fluids 39 (2005) 364–374.
[16] M. Pasandideh-Fard, S.D. Aziz, S. Chandra, J. Mostaghimi, Cooling effectiveness of a water drop impinging on a hot surface, Int. J. Heat. Fluid Flow. 22 (2001) 201–210.
[17] W. Cheng, W. Zhang, H. Chen, L. Hu, Spray cooling and flash evaporation cooling: the current development and application, Renew. Sustain. Energy Rev. 55 (2016) 614–628.
[18] G. Liang, I. Mudawar, Review of spray cooling – Part 1: single-phase and nucleate boiling regimes, and critical heat flux, Int. J. Heat. Mass Transf. 115 (2017) 1174–1205.
[19] G. Liang, I. Mudawar, Review of spray cooling – Part 2: high temperature boiling regimes and quenching applications, Int. J. Heat. Mass Transf. 115 (2017) 1206–1222.
[20] A.L.N. Moreira, A.S. Moita, M.R. Panão, Advances and challenges in explaining fuel spray impingement: How much of single droplet impact research is useful? Prog. Energy Combust. Sci. 36 (2010) 554–580.
[21] T. Young, An essay on the cohesion of fluids, Philos. Trans. R. Soc. Lond. 95 (1805) 65–87.
[22] Q. Jiang, H.M. Lu, Size dependent interface energy and its applications, Surf. Sci. Rep. 63 (2008) 427–464.
[23] A.K. Kota, G. Kwon, A. Tuteja, The design and applications of superomniphobic surfaces, NPG Asia Mater. 6 (2014), e109.
[24] P. Muthiah, B. Bhushan, K. Yun, H. Kondo, Dual-layered-coated mechanically-durable superomniphobic surfaces with anti-smudge properties, J. Colloid Interface Sci. 409 (2013) 227–236.
[25] E.F. Hare, E.G. Shafrin, W.A. Zisman, Properties of films of adsorbed fluorinated acids, J. Phys. Chem. 58 (1954) 236–239.
[26] J. Genzer, K. Efimenko, Creating long-lived superhydrophobic polymer surfaces through mechanically assembled monolayers, Science 290 (2000) 2130–2133.
[27] T. Nishino, M. Meguro, K. Nakamae, M. Matsushita, Y. Ueda, The lowest surface free energy based on -CF3 alignment, Langmuir 15 (1999) 4321–4323.
[28] A.K. Kota, W. Choi, A. Tuteja, Superomniphobic surfaces: design and durability, MRS Bull. 38 (2013) 383–390.
[29] W. Li, M. Yu, J. Sun, K. Mochizuki, S. Chen, H. Zheng, J. Li, S. Yao, H. Wu, B. S. Ong, S. Kawata, Z. Wang, K. Ren, Crack engineering for the construction of arbitrary hierarchical architectures, Proc. Natl. Acad. Sci. U. S. A. 116 (2019) 23909–23914.
[30] D. Wang, Q. Sun, M.J. Hokkanen, C. Zhang, F.Y. Lin, Q. Liu, S.P. Zhu, T. Zhou, Q. Chang, B. He, Q. Zhou, L. Chen, Z. Wang, R.H.A. Ras, X. Deng, Design of robust superhydrophobic surfaces, Nature 582 (2020) 55–59.
[31] F. Celestini, G. Kirstetter, Effect of an electric field on a Leidenfrost droplet, Soft Matter 8 (2012) 5992–5995.
[32] J.C. Burton, A.L. Sharpe, R.C.A. Van Der Veen, A. Franco, S.R. Nagel, Geometry of the vapor layer under a Leidenfrost drop, Phys. Rev. Lett. 109 (2012) 1–4.
[33] T. Tran, H.J.J. Staat, A. Prosperetti, C. Sun, D. Lohse, Drop impact on superheated surfaces, Phys. Rev. Lett. 108 (2012) 1–5.
[34] M. Shirota, M.A.J. Van Limbeek, C. Sun, A. Prosperetti, D. Lohse, Dynamic Leidenfrost effect: relevant time and length scales, Phys. Rev. Lett. 116 (2016) 1–5.
[35] M. Khavari, C. Sun, D. Lohse, T. Tran, Fingering patterns during droplet impact on heated surfaces, Soft Matter 11 (2015) 3298–3303.

[36] J.E. Sprittles, Y.D. Shikhmurzaev, The dynamics of liquid drops and their interaction with solids of varying wettabilities, Phys. Fluids 24 (2012), 082001.
[37] P.G. Bange, R. Bhardwaj, Computational study of bouncing and non-bouncing droplets impacting on superhydrophobic surfaces, Theor. Comput. Fluid Dyn. 30 (2016) 211–235.
[38] H. Shetabivash, A. Dolatabadi, Numerical investigation of air mediated droplet bouncing on flat surfaces, AIP Adv. 7 (2017), 095003.
[39] Y. Quan, L.Z. Zhang, Numerical and analytical study of the impinging and bouncing phenomena of droplets on superhydrophobic surfaces with microtextured structures, Langmuir 30 (2014) 11640–11649.
[40] M.L.D. Bothe, Toward the predictive simulation of bouncing versus coalescence in binary droplet collisions, Acta Mech. 230 (2019) 623–644.
[41] P. Pournaderi, A.R. Pishevar, A numerical investigation of droplet impact on a heated wall in the film boiling regime, Heat. Mass Transf. 48 (2012) 1525–1538.
[42] D. Caviezel, C. Narayanan, D. Lakehal, Adherence and bouncing of liquid droplets impacting on dry surfaces, Microfluid. Nanofluid. 5 (2008) 469–478.
[43] D. Khojasteh, A. Bordbar, R. Kamali, M. Marengo, Curvature effect on droplet impacting onto hydrophobic and superhydrophobic spheres, Int. J. Comput. Fluid Dyn. 31 (2017) 310–323.
[44] K. Yokoi, D. Vadillo, J. Hinch, I. Hutchings, Numerical studies of the influence of the dynamic contact angle on a droplet impacting on a dry surface, Phys. Fluids 21 (2009), 072102.
[45] Z. Shusheng, L. Hao, Z. Li-Zhi, R. Saffa, U. Zafer, Z. Huaguan, A lattice Boltzmann simulation of oblique impact of a single rain droplet on super-hydrophobic surface with randomly distributed rough structures, Int. J. Low. Carbon Tec. 15 (2020) 443–449.
[46] W.Z. Yuan, L.Z. Zhang, Lattice Boltzmann simulation of droplets impacting on superhydrophobic surfaces with randomly distributed rough structures, Langmuir 33 (2017) 820–829.
[47] C. Yin, T. Wang, Z. Che, M. Jia, K. Sun, Oblique impact of droplets on microstructured superhydrophobic surfaces, Int. J. Heat. Mass Transf. 123 (2018) 693–704.
[48] L. Moevius, Y. Liu, Z. Wang, J.M. Yeomans, Pancake bouncing: simulations and theory and experimental verification, Langmuir 30 (2014) 13021–13032.
[49] T. Koishi, K. Yasuoka, X.C. Zeng, Molecular dynamics simulation of water nanodroplet bounce back from flat and nanopillared surface, Langmuir 33 (2017) 10184–10192.
[50] S. Gao, Q. Liao, W. Liu, Z. Liu, Coalescence-induced jumping of nanodroplets on textured surfaces, J. Phys. Chem. Lett. 9 (2018) 13–18.
[51] S. Gao, Q. Liao, W. Liu, Z. Liu, Self-removal of multiple and multisize coalescing nanodroplets on nanostructured surfaces, J. Phys. Chem. C. 122 (2018) 20521–20526.
[52] S. Gao, Q. Liao, W. Liu, Z. Liu, Nanodroplets impact on rough surfaces: a simulation and theoretical study, Langmuir 34 (2018) 5910–5917.
[53] H.Y. Lo, Y. Liu, L. Xu, Mechanism of contact between a droplet and an atomically smooth substrate, Phys. Rev. X 7 (2017) 1–14.
[54] L. Chen, J. Wu, Z. Li, S. Yao, Evolution of entrapped air under bouncing droplets on viscoelastic surfaces, Colloids Surf. A Physicochem. Eng. Asp. 384 (2011) 726–732.
[55] J.C. Bird, R. Dhiman, H.M. Kwon, K.K. Varanasi, Reducing the contact time of a bouncing drop, Nature 503 (2013) 385–388.
[56] Y. Shen, J. Tao, H. Tao, S. Chen, L. Pan, T. Wang, Relationship between Wetting hysteresis and contact time of a bouncing droplet on hydrophobic surfaces, ACS Appl. Mater. Interfaces 7 (2015) 20972–20978.
[57] Y. Shen, J. Tao, H. Tao, S. Chen, L. Pan, T. Wang, Approaching the theoretical contact time of a bouncing droplet on the rational macrostructured superhydrophobic surfaces, Appl. Phys. Lett. 107 (2015), 111604.
[58] Y. Liu, M. Andrew, J. Li, J.M. Yeomans, Z. Wang, Symmetry breaking in drop bouncing on curved surfaces, Nat. Commun. 6 (2015) 10034.
[59] M. Andrew, Y. Liu, J.M. Yeomans, Variation of the contact time of droplets bouncing on cylindrical ridges with ridge size, Langmuir 33 (2017) 7583–7587.
[60] Y. Liu, L. Moevius, X. Xu, T. Qian, J.M. Yeomans, Z. Wang, Pancake bouncing on superhydrophobic surfaces, Nat. Phys. 10 (2014) 515–519.
[61] Y. Liu, G. Whyman, E. Bormashenko, C. Hao, Z. Wang, Controlling drop bouncing using surfaces with gradient features, Appl. Phys. Lett. 107 (2015) 0–5.
[62] Y. Liu, Z. Wang, Superhydrophobic porous networks for enhanced droplet shedding, Sci. Rep. 6 (2016) 1–7.
[63] B. Zhang, Q. Lei, Z. Wang, X. Zhang, Droplets can rebound toward both directions on textured surfaces with a wettability gradient, Langmuir 32 (2016) 346–351.
[64] H. Li, W. Fang, Y. Li, Q. Yang, M. Li, Q. Li, X.Q. Feng, Y. Song, Spontaneous droplets gyrating via asymmetric self-splitting on heterogeneous surfaces, Nat. Commun. 10 (2019) 1–6.
[65] T.M. Schutzius, S. Jung, T. Maitra, G. Graeber, M. Köhme, D. Poulikakos, Spontaneous droplet trampolining on rigid superhydrophobic surfaces, Nature 527 (2015) 82–85.
[66] J. De Ruiter, R. Lagraauw, D. Van Den Ende, F. Mugele, Wettability-independent bouncing on flat surfaces mediated by thin air films, Nat. Phys. 11 (2015) 48–53.
[67] J. De Ruiter, R. Lagraauw, F. Mugele, D. Van Den Ende, Bouncing on thin air: how squeeze forces in the air film during non-wetting droplet bouncing lead to momentum transfer and dissipation, J. Fluid Mech. 776 (2015) 531–567.
[68] J.M. Kolinski, L. Mahadevan, S.M. Rubinstein, Drops can bounce from perfectly hydrophilic surfaces, Epl 108 (2014) 24001.
[69] J.G. Leidenfrost, On the fixation of water in diverse fire, Int. J. Heat. Mass Transf. 9 (1966) 1153–1166.
[70] S. Lyu, V. Mathai, Y. Wang, B. Sobac, P. Colinet, D. Lohse, C. Sun, Final fate of a Leidenfrost droplet: explosion or take off, Sci. Adv. 5 (2019) 1–7.
[71] G. Liang, S. Shen, Y. Guo, J. Zhang, Boiling from liquid drops impact on a heated wall, Int. J. Heat. Mass Transf. 100 (2016) 48–57.
[72] T. Tran, H.J.J. Staat, A. Susarrey-Arce, T.C. Foertsch, A. van Houselt, H.J.G. E. Gardeniers, A. Prosperetti, D. Lohse, C. Sun, Droplet impact on superheated micro-structured surfaces, Soft Matter 9 (2013) 3272–3282.
[73] J.H. Snoeijer, P. Brunet, J. Eggers, Maximum size of drops levitated by an air cushion, Phys. Rev. E 79 (2009) 1–13.
[74] J.H. Moon, D.Y. Kim, S.H. Lee, Spreading and receding characteristics of a non-Newtonian droplet impinging on a heated surface, Exp. Therm. Fluid Sci. 57 (2014) 94–101.
[75] G. Castanet, O. Caballina, F. Lemoine, Drop spreading at the impact in the Leidenfrost boiling, Phys. Fluids 27 (2015), 063302.
[76] V.E. Nakoryakov, S.Y. Misyura, S.L. Elistratov, The behavior of water droplets on the heated surface, Int. J. Heat. Mass Transf. 55 (2012) 6609–6617.
[77] M.A.J. Van Limbeek, M. Shirota, P. Sleutel, C. Sun, A. Prosperetti, D. Lohse, Vapour cooling of poorly conducting hot substrates increases the dynamic Leidenfrost temperature, Int. J. Heat. Mass Transf. 97 (2016) 101–109.
[78] H.M. Kwon, J.C. Bird, K.K. Varanasi, Increasing Leidenfrost point using micro-nano hierarchical surface structures, Appl. Phys. Lett. 103 (2013), 201601.
[79] C. Kruse, T. Anderson, C. Wilson, C. Zuhlke, D. Alexander, G. Gogos, S. Ndao, Extraordinary shifts of the leidenfrost temperature from multiscale micro/nanostructured surfaces, Langmuir 29 (2013) 9798–9806.
[80] H. Nair, H.J.J. Staat, T. Tran, A. van Houselt, A. Prosperetti, D. Lohse, C. Sun, The Leidenfrost temperature increase for impacting droplets on carbon-nanofiber surfaces, Soft Matter 10 (2014) 2102–2109.
[81] E.S.R. Negeed, M. Albeirutty, Y. Takata, Dynamic behavior of micrometric single water droplets impacting onto heated surfaces with TiO_2 hydrophilic coating, Int. J. Therm. Sci. 79 (2014) 1–17.
[82] D. Arnaldo del Cerro, Á.G. Marín, G.R.B.E. Römer, B. Pathiraj, D. Lohse, A.J. Huis in 't Veld, Leidenfrost point reduction on micropatterned metallic surfaces, Langmuir 28 (2012) 15106–15110.
[83] C.M. Weickgenannt, Y. Zhang, S. Sinha-Ray, I.V. Roisman, T. Gambaryan-Roisman, C. Tropea, A.L. Yarin, Inverse-Leidenfrost phenomenon on nanofiber mats on hot surfaces. Phys. Rev. E Stat. Nonlinear Soft Matter Phys. 84 (2011) 1–9.
[84] L. Maquet, M. Brandenbourger, B. Sobac, A.L. Biance, P. Colinet, S. Dorbolo, Leidenfrost drops: effect of gravity, Europhys. Lett. 110 (2015) 24001.
[85] B.T. Ng, Y.M. Hung, M.K. Tan, Suppression of the Leidenfrost effect via low frequency vibrations, Soft Matter 11 (2015) 775–784.
[86] D. Orejon, K. Sefiane, Y. Takata, Effect of ambient pressure on Leidenfrost temperature, Phys. Rev. E 90 (2014) 1–6.
[87] M.A.J. Van Limbeek, P.B.J. Hoefnagels, M. Shirota, C. Sun, D. Lohse, Boiling regimes of impacting drops on a heated substrate under reduced pressure, Phys. Rev. Fluids 3 (2018), 053601.
[88] R.L. Agapov, J.B. Boreyko, D.P. Briggs, B.R. Srijanto, S.T. Retterer, C.P. Collier, N. V. Lavrik, Asymmetric wettability of nanostructures directs Leidenfrost droplets, ACS Nano 8 (2014) 860–867.
[89] P. Zhang, B. Peng, J. Wang, L. Jiang, Bioinspired self-propulsion of water droplets at the convergence of janus-textured heated substrates, Adv. Funct. Mater. 29 (2019) 1–8.
[90] J. Li, Y. Hou, Y. Liu, C. Hao, M. Li, M.K. Chaudhury, S. Yao, Z. Wang, Directional transport of high-temperature Janus droplets mediated by structural topography, Nat. Phys. 12 (2016) 606–612.
[91] P. Testa, L. Nicotra, Influence of pressure on the leidenfrost temperature and on extracted heat fluxes in the transient mode and low pressure, J. Heat. Transf. 108 (1986) 916–921.
[92] G.S. Emmerson, The effect of pressure and surface material on the leidenfrost point of discrete drops of water, Int. J. Heat. Mass Transf. 18 (1975) 381–386.
[93] F. Celestini, T. Frisch, Y. Pomeau, Room temperature water Leidenfrost droplets, Soft Matter 9 (2013) 9535.
[94] X. Yu, R. Hu, X. Zhang, B. Xie, X. Luo, Explosive bouncing on heated silicon surfaces under low ambient pressure, Soft Matter 15 (2019) 4320–4325.
[95] Y. Couder, E. Fort, C.H. Gautier, A. Boudaoud, From bouncing to floating: noncoalescence of drops on a fluid bath, Phys. Rev. Lett. 94 (2005) 1–4.
[96] S. Sikalo, C. Tropea, E.N. Ganić, Impact of droplets onto inclined surfaces, J. Colloid Interface Sci. 286 (2005) 661–669.
[97] C. Hao, J. Li, Y. Liu, X. Zhou, Y. Liu, R. Liu, L. Che, W. Zhou, D. Sun, L. Li, L. Xu, Z. Wang, Superhydrophobic-like tunable droplet bouncing on slippery liquid interfaces, Nat. Commun. 6 (2015) 1–7.
[98] T. Gilet, J.W.M. Bush, Droplets bouncing on a wet, inclined surface, Phys. Fluids 24 (2012), 122103.
[99] G. Liang, Y. Yang, Y. Guo, N. Zhen, S. Shen, Rebound and spreading during a drop impact on wetted cylinders, Exp. Therm. Fluid Sci. 52 (2014) 97–103.
[100] Y.K. Cai, Phenomena of a liquid drop falling to a liquid surface, Exp. Fluids 7 (1989) 388–394.
[101] Ø. Wind-Willassen, J. Moláček, D.M. Harris, J.W.M. Bush, Exotic states of bouncing and walking droplets, Phys. Fluids 25 (2013), 082002.
[102] R.N. Valani, A.C. Slim, T. Simula, Superwalking droplets, Phys. Rev. Lett. 123 (2019), 024503.
[103] D. Terwagne, F. Ludewig, N. Vandewalle, S. Dorbolo, The role of the droplet deformations in the bouncing droplet dynamics, Phys. Fluids 25 (2013), 122101.
[104] S.E. Turton, M.M.P. Couchman, J.W.M. Bush, A review of the theoretical modeling of walking droplets: Toward a generalized pilot-wave framework, Chaos 28 (2018), 096111.
[105] J.W.M. Bush, Pilot-wave hydrodynamics, Annu. Rev. Fluid Mech. 47 (2015) 269–292.

[106] Y.J. Jiang, A. Umemura, C.K. Law, An experimental investigation on the collision behaviour of hydrocarbon droplets, J. Fluid Mech. 234 (1992) 171–190.
[107] K. Willis, M. Orme, Binary droplet collisions in a vacuum environment: an experimental investigation of the role of viscosity, Exp. Fluids 34 (2003) 28–41.
[108] J.-P. Estrade, H. Carentz, G. Lavergne, Y. Biscos, Experimental investigation of dynamic binary collision of ethanol droplets – a model for droplet coalescence and bouncing, Int. J. Heat. Fluid Flow. 20 (1999) 486–491.
[109] M. Orme, Experiments on droplet collisions, bounce, coalescence and disruption, Prog. Energy Combust. Sci. 23 (1997) 65–79.
[110] K.-L. Pan, C.K. Law, B. Zhou, Experimental and mechanistic description of merging and bouncing in head-on binary droplet collision, J. Appl. Phys. 103 (2008), 064901.
[111] N.J. Cira, A. Benusiglio, M. Prakash, Vapour-mediated sensing and motility in two-component droplets, Nature 519 (2015) 446–450.
[112] R.-H. Chen, C.-T. Chen, Collision between immiscible drops with large surface tension difference: diesel oil and water, Exp. Fluids 41 (2006) 453–461.
[113] W.D. Ristenpart, J.C. Bird, A. Belmonte, F. Dollar, H.A. Stone, Non-coalescence of oppositely charged drops, Nature 461 (2009) 377–380.
[114] N. Yi, B. Huang, L. Dong, X. Quan, F. Hong, P. Tao, C. Song, W. Shang, T. Deng, Temperature-induced coalescence of colliding binary droplets on superhydrophobic surface, Sci. Rep. 4 (2014) 4303.
[115] M. Damak, K. Varanasi, Expansion and retraction dynamics in drop-on-drop impacts on nonwetting surfaces, Phys. Rev. Fluids 3 (2018) 1–12.
[116] S. Helmensdorfer, P. Topping, Bouncing of charged droplets: an explanation using mean curvature flow, Epl 104 (2013) 34001.
[117] H. Xu, C. Chang, N. Yi, P. Tao, C. Song, J. Wu, T. Deng, W. Shang, Coalescence, spreading, and rebound of two water droplets with different temperatures on a superhydrophobic surface, ACS Omega 4 (2019) 17615–17622.
[118] H. Mertaniemi, R. Forchheimer, O. Ikkala, R.H.A. Ras, Rebounding droplet-droplet collisions on superhydrophobic surfaces: from the phenomenon to droplet logic, Adv. Mater. 24 (2012) 5738–5743.
[119] S. Pan, R. Guo, J.J. Richardson, J.D. Berry, Q.A. Besford, M. Björnmalm, G. Yun, R. Wu, Z. Lin, Q.Z. Zhong, J. Zhou, Q. Sun, J. Li, Y. Lu, Z. Dong, M.K. Banks, W. Xu, J. Jiang, L. Jiang, F. Caruso, Ricocheting Droplets Moving on Super-Repellent Surfaces, Adv. Sci. 6 (2019), 1901846.
[120] H. Vahabi, W. Wang, J.M. Mabry, A.K. Kota, Coalescence-induced jumping of droplets on superomniphobic surfaces with macrotexture, Sci. Adv. 4 (2018) 1–8.
[121] R. Mukherjee, A.S. Berrier, K.R. Murphy, J.R. Vieitez, J.B. Boreyko, How surface orientation affects jumping-droplet condensation, Joule 3 (2019) 1360–1376.
[122] N. Miljkovic, D.J. Preston, R. Enright, E.N. Wang, Electrostatic charging of jumping droplets, Nat. Commun. 4 (2013) 1–9.
[123] C. Stamatopoulos, A. Milionis, N. Ackerl, M. Donati, P. Leudet de la Vallée, P. Rudolf von Rohr, D. Poulikakos, Droplet self-propulsion on superhydrophobic microtracks, ACS Nano 14 (2020) 12895–12904, https://doi.org/10.1021/acsnano.0c03849.
[124] K. Golovin, A. Dhyani, M.D. Thouless, A. Tuteja, Low-interfacial toughness materials for effective large-scale deicing, Sci. (80-.) 364 (2019) 371–375.
[125] S. Jung, M.K. Tiwari, N.V. Doan, D. Poulikakos, Mechanism of supercooled droplet freezing on surfaces, Nat. Commun. 3 (2012) 615.
[126] S. Movafaghi, W. Wang, A. Metzger, D.D. Williams, J.D. Williams, A.K. Kota, Tunable superomniphobic surfaces for sorting droplets by surface tension, Lab Chip 16 (2016) 3204–3209.
[127] J. Li, X. Zhou, J. Li, L. Che, J. Yao, G. McHale, M.K. Chaudhury, Z. Wang, Topological liquid diode, Sci. Adv. 3 (2017) 19–25.
[128] L. Wang, C. Gao, Y. Hou, Y. Zheng, L. Jiang, Magnetic field-guided directional rebound of a droplet on a superhydrophobic flexible needle surface, J. Mater. Chem. A 4 (2016) 18289–18293.
[129] T.A. Duncombe, E.Y. Erdem, A. Shastry, R. Baskaran, K.F. Böhringer, Controlling liquid drops with texture ratchets, Adv. Mater. 24 (2012) 1545–1550.
[130] R.L. Agapov, J.B. Boreyko, D.P. Briggs, B.R. Srijanto, S.T. Retterer, C.P. Collier, N. V. Lavrik, Length scale selects directionality of droplets on vibrating pillar ratchet, Adv. Mater. Interfaces 1 (2014) 1–8.
[131] T.R. Cousins, R.E. Goldstein, J.W. Jaworski, A.I. Pesci, A ratchet trap for Leidenfrost drops, J. Fluid Mech. 696 (2012) 215–227.
[132] Á.G. Marín, D. Arnaldo del Cerro, G.R.B.E. Römer, B. Pathiraj, A. Huis in't Veld, D. Lohse, Capillary droplets on Leidenfrost micro-ratchets, Phys. Fluids 24 (2012), 122001.
[133] G. Lagubeau, M. Le Merrer, C. Clanet, D. Quéré, Leidenfrost on a ratchet, Nat. Phys. 7 (2011) 395–398.
[134] G. Dupeux, P. Bourrianne, Q. Magdelaine, C. Clanet, D. Quéré, Propulsion on a superhydrophobic ratchet, Sci. Rep. 4 (2014).
[135] Z. hai Jia, M. yao Chen, H. tao Zhu, Reversible self-propelled Leidenfrost droplets on ratchet surfaces, Appl. Phys. Lett. 110 (2017), 091603.
[136] C. Kruse, I. Somanas, T. Anderson, C. Wilson, C. Zuhlke, D. Alexander, G. Gogos, S. Ndao, Self-propelled droplets on heated surfaces with angled self-assembled micro/nanostructures, Microfluid. Nanofluid. 18 (2015) 1417–1424.
[137] H. Linke, B.J. Alemán, L.D. Melling, M.J. Taormina, M.J. Francis, C.C. Dow-Hygelund, V. Narayanan, R.P. Taylor, A. Stout, Self-propelled leidenfrost droplets, Phys. Rev. Lett. 96 (2006) 2–5.
[138] J.M. Arter, D.J. Cleaver, K. Takashina, A.T. Rhead, Self-propelling Leidenfrost droplets on a variable topography surface, Appl. Phys. Lett. 113 (2018) 1–6.
[139] G. Dupeux, M. Le Merrer, G. Lagubeau, C. Clanet, S. Hardt, D. Quéré, Viscous mechanism for Leidenfrost propulsion on a ratchet, Europhys. Lett. 96 (2011) 58001.
[140] Q. Li, Q.J. Kang, M.M. Francois, A.J. Hu, Lattice Boltzmann modeling of self-propelled Leidenfrost droplets on ratchet surfaces, Soft Matter 20 (2016) 993–1001.
[141] S. Feng, J. Delannoy, A. Malod, H. Zheng, D. Quéré, Z. Wang, Tip-induced flipping of droplets on Janus pillars: From local reconfiguration to global transport, Sci. Adv. 6 (2020) 1–7.
[142] J. Li, N.S. Ha, T. "Leo" Liu, R.M. van Dam, "CJ", C.J. Kim, Ionic-surfactant-mediated electro-dewetting for digital microfluidics, Nature 572 (2019) 507–510.
[143] S. Lee, S. Lee, H. Hwang, J. Hong, S. Lee, J. Lee, Y. Chae, T. Lee, Ultrafast single-droplet bouncing actuator with electrostatic force on superhydrophobic electrodes, RSC Adv. 6 (2016) 66729–66737.
[144] Q. Sun, D. Wang, Y. Li, J. Zhang, S. Ye, J. Cui, L. Chen, Z. Wang, H.J. Butt, D. Vollmer, X. Deng, Surface charge printing for programmed droplet transport, Nat. Mater. 18 (2019) 936–941.
[145] X. Wang, Y. Liu, Y. Zhang, Velocity difference of aqueous drops bouncing between parallel electrodes, J. Dispers. Sci. Technol. 36 (2014).
[146] G.M. Whitesides, The origins and the future of microfluidics, Nature 442 (2006) 368–373.
[147] M. Prakash, N. Gershenfeld, Microfluidic bubble logic, Sci. (80-.) 315 (2007) 832–835.
[148] G. Katsikis, J.S. Cybulski, M. Prakash, Synchronous universal droplet logic and control, Nat. Phys. 11 (2015) 588–596.
[149] F.G. Woodhouse, J. Dunkel, Active matter logic for autonomous microfluidics, Nat. Commun. 8 (2017) 1–7.
[150] L.F. Cheow, L. Yobas, D.L. Kwong, Digital microfluidics: Droplet based logic gates, Appl. Phys. Lett. 90 (2007) 1–4.
[151] N. Vourdas, D.C. Moschou, K.A. Papadopoulos, D. Davazoglou, V.N. Stathopoulos, A new microfluidic pressure-controlled field effect transistor (pFET) in digital fluidic switch operation mode, Microelectron. Eng. 190 (2018) 28–32.
[152] B. Zhou, L. Wang, S. Li, X. Wang, Y.S. Hui, W. Wen, Universal logic gates via liquid-electronic hybrid divider, Lab Chip 12 (2012) 5211–5217.
[153] M.W. Toepke, V.V. Abhyankar, D.J. Beebe, Microfluidic logic gates and timers, Lab Chip 7 (2007) 1449–1453.
[154] T.C. Draper, C. Fullarton, N. Phillips, B.P.J. de Lacy Costello, A. Adamatzky, Liquid marble interaction gate for collision-based computing, Mater. Today 20 (2017) 561–568.
[155] J. Yin, Z. Zhang, X. Li, J. Yu, J. Zhou, Y. Chen, W. Guo, Waving potential in graphene, Nat. Commun. 5 (2014) 3582.
[156] J. Yin, X. Li, J. Yu, Z. Zhang, J. Zhou, W. Guo, Generating electricity by moving a droplet of ionic liquid along graphene, Nat. Nanotechnol. 9 (2014) 378–383.
[157] Z. Zhang, X. Li, J. Yin, Y. Xu, W. Fei, M. Xue, Q. Wang, J. Zhou, W. Guo, Emerging hydrovoltaic technology, Nat. Nanotechnol. 13 (2018) 1109–1119.
[158] J. Yin, J. Zhou, S. Fang, W. Guo, Hydrovoltaic energy on the way, Joule 4 (2020) 1852–1855.
[159] Z.H. Lin, G. Cheng, S. Lee, K.C. Pradel, Z.L. Wang, Harvesting water drop energy by a sequential contact-electrification and electrostatic-induction process, Adv. Mater. 26 (2014) 4690–4696.
[160] Z.H. Lin, G. Cheng, L. Lin, S. Lee, Z.L. Wang, Water-solid surface contact electrification and its use for harvesting liquid-wave energy, Angew. Chem. Int. Ed. 52 (2013) 12545–12549.
[161] S.S. Kwak, S. Lin, J.H. Lee, H. Ryu, T.Y. Kim, H. Zhong, H. Chen, S.W. Kim, Triboelectrification-induced large electric power generation from a single moving droplet on graphene/polytetrafluoroethylene, ACS Nano 10 (2016) 7297–7302.
[162] L. Zheng, Z.H. Lin, G. Cheng, W. Wu, X. Wen, S. Lee, Z.L. Wang, Silicon-based hybrid cell for harvesting solar energy and raindrop electrostatic energy, Nano Energy 9 (2014) 291–300.
[163] W. Xu, H. Zheng, Y. Liu, X. Zhou, C. Zhang, Y. Song, X. Deng, M. Leung, Z. Yang, R.X. Xu, Z.L. Wang, X.C. Zeng, Z. Wang, A droplet-based electricity generator with high instantaneous power density, Nature 578 (2020) 392–396.
[164] H. Wu, N. Mendel, S. van der Ham, L. Shui, G. Zhou, F. Mugele, Charge trapping-based electricity generator (CTEG): an ultrarobust and high efficiency nanogenerator for energy harvesting from water droplets, Adv. Mater. (2020), https://doi.org/10.1002/adma.202001699.
[165] H. Wu, N. Mendel, D. van den Ende, G. Zhou, F. Mugele, Energy harvesting from drops impacting onto charged surfaces, Phys. Rev. Lett. 125 (2020), 078301.
[166] S. Wang, L. Lin, Z.L. Wang, Nanoscale triboelectric-effect-enabled energy conversion for sustainably powering portable electronics, Nano Lett. 12 (2012) 6339–6346.
[167] G. Zhu, Z.H. Lin, Q. Jing, P. Bai, C. Pan, Y. Yang, Y. Zhou, Z.L. Wang, Toward large-scale energy harvesting by a nanoparticle-enhanced triboelectric nanogenerator, Nano Lett. 13 (2013) 847–853.
[168] J. Nie, Z. Wang, Z. Ren, S. Li, X. Chen, Z. Lin Wang, Power generation from the interaction of a liquid droplet and a liquid membrane, Nat. Commun. 10 (2019) 1–10.
[169] G. Xue, Y. Xu, T. Ding, J. Li, J. Yin, W. Fei, Y. Cao, J. Yu, L. Yuan, L. Gong, J. Chen, S. Deng, J. Zhou, W. Guo, Water-evaporation-induced electricity with nanostructured carbon materials, Nat. Nanotechnol. 12 (2017) 317–321.
[170] G. Zhu, Y. Su, P. Bai, J. Chen, Q. Jing, W. Yang, Z.L. Wang, Harvesting water wave energy by asymmetric screening of electrostatic charges on a nanostructured hydrophobic thin-film surface, ACS Nano 8 (2014) 6031–6037.
[171] J. Yu, T. Ma, Triboelectricity-based self-charging droplet capacitor for harvesting low-level ambient energy, Nano Energy 74 (2020), 104795.
[172] Y. Chen, Y. Kuang, D. Shi, M. Hou, X. Chen, L. Jiang, J. Gao, L. Zhang, Y. He, C. P. Wong, A triboelectric nanogenerator design for harvesting environmental mechanical energy from water mist, Nano Energy 73 (2020), 104765.

[173] D. Jiang, Y. Su, K. Wang, Y. Wang, M. Xu, M. Dong, G. Chen, A triboelectric and pyroelectric hybrid energy harvester for recovering energy from low-grade waste fluids, Nano Energy 70 (2020), 104459.
[174] X. Jiao, S. Yang, Z. Lin, G. Zhu, Electricity−free electroluminescence excited by droplet impact driven triboelectric field on solid−liquid interface, Nano Energy 75 (2020), 104823.
[175] J. Li, K. Liu, G. Xue, T. Ding, P. Yang, Q. Chen, Y. Shen, S. Li, G. Feng, A. Shen, M. Xu, J. Zhou, Electricity generation from water droplets via capillary in fi ltrating, Nano Energy 48 (2018) 211–216.
[176] Y. Yang, J. Park, S. Geun, Y. Sang, Electricity modulation of a water motion active transducer via surface functionality control, Nano Energy 40 (2017) 447–453.
[177] A.S. Aji, R. Nishi, H. Ago, Y. Ohno, High output voltage generation of over 5 V from liquid motion on single-layer MoS_2, Nano Energy 68 (2020), 104370.
[178] P. Cui, J. Wang, J. Xiong, S. Li, W. Zhang, X. Liu, G. Gu, J. Guo, B. Zhang, G. Cheng, Z. Du, Meter-scale fabrication of water-driven triboelectric nanogenerator based on in-situ grown layered double hydroxides through a bottom-up approach, Nano Energy 71 (2020), 104646.
[179] Y. Wang, J. Duan, Y. Zhao, Y. Duan, Q. Tang, Self-powered PEDOT and derivate monoelectrodes to harvest rain energy, Nano Energy 41 (2017) 293–300.
[180] H. Cho, J. Chung, G. Shin, J.Y. Sim, D.S. Kim, S. Lee, W. Hwang, Toward sustainable output generation of liquid – solid contact triboelectric nanogenerators: the role of hierarchical structures, Nano Energy 56 (2019) 56–64.
[181] D. Park, S. Won, K. Kim, J. Jung, J. Choi, The influence of substrate-dependent triboelectric charging of graphene on the electric potential generation by the fl ow of electrolyte droplets, Nano Energy 54 (2018) 66–72.
[182] Y. Luo, Y. Li, X. Feng, Y. Pei, Z. Zhang, L. Wang, Y. Zhao, B. Lu, B. Zhu, Triboelectric nanogenerators with porous and hierarchically structured silk fibroin films via water electrospray-etching technology, Nano Energy 75 (2020), 104974.
[183] C. Park, S. Yu, S.M. Cho, G. Song, Y. Lee, H.S. Kang, S.W. Lee, H. Eoh, C. Park, Triboelectric nanogenerators with transfer-printed arrays of hierarchically dewetted microdroplets, Nano Energy 51 (2018) 588–596.
[184] J.H. Lee, S. Kim, T.Y. Kim, U. Khan, S. Kim, Water droplet-driven triboelectric nanogenerator with superhydrophobic surfaces, Nano Energy 58 (2019) 579–584.
[185] Y. Wang, Y. Yang, Superhydrophobic surfaces-based redox-induced electricity from water droplets for self-powered wearable electronics, Nano Energy 56 (2019) 547–554.
[186] W. Tang, B.D. Chen, Z.L. Wang, Recent progress in power generation from water/liquid droplet interaction with solid surfaces, Adv. Funct. Mater. 29 (2019) 1–13.
[187] Y. Wang, S. Gao, W. Xu, Z. Wang, Nanogenerators with superwetting surfaces for harvesting water/liquid energy, Adv. Funct. Mater. 30 (2020) 1–15.